Functional Anatomy and Evolution of a Novel Skeletal Element in Bat Feet

Kathryn E. Stanchak

A dissertation

submitted in partial fulfillment of the

requirements for the degree of

Doctor of Philosophy

University of Washington

2019

Reading Committee:

Sharlene E. Santana Mata, Chair

Susan W. Herring

Adam P. Summers

Program Authorized to Offer Degree:

Biology

University of Washington

Abstract

Functional Anatomy and Evolution of a Novel Skeletal Element in Bat Feet

Kathryn E. Stanchak

Chair of the Supervisory Committee:
Sharlene E. Santana
Department of Biology

The striking postcranial anatomy of bats reflects their specialized ecology; they are the only mammals capable of powered flight. Bat postcranial adaptations include a series of membranes that connect highly-modified, or even novel, skeletal elements. While most studies of bat postcranial anatomy have focused on their wings, bat hindlimbs also contain many derived and functionally important, yet less studied, features. In this study, I investigate the anatomy, evolution, and function of the calcar, a novel skeletal element found in bat feet. In the first chapter, I introduce calcar anatomy with a detailed study of three bat species with different flight and foraging ecologies. I found more complex muscle arrangements in the species that exhibit more maneuverable flight, suggesting that they have more control over calcar movement. This first study inspired the rest of the dissertation, by suggesting that calcar morphology is functionally-relevant. In the second chapter, I present a thorough overview of calcar skeletal anatomy throughout Chiroptera. Through evolutionary modeling of calcar length, I find that the calcar exhibits an early burst of morphological evolution, indicating that the calcar anatomically diversified as bats initially radiated through the aerosphere. In the third chapter, I again narrow

the focus and conduct an analysis of calcar motion during free, forward-flight in a laboratory population of Seba's short-tailed fruit bat (*Carollia perspicillata*). I find that the calcar does rotate about its joint with the calcaneus and that this rotation is greater about one axis than another. The muscles inserting on the calcar may act to stabilize it in one plane of motion. These chapters provide the most complete study of calcars to-date, particularly with regard to the quantitative tests of calcar evolutionary patterns and kinematics. Four data tables and one video are provided as Electronic Supplementary Materials for Chapters 2 and 3. Collectively, these three chapters demonstrate that novel skeletal additions can become integrated into vertebrate body plans and subsequently evolve into a variety of forms, potentially impacting clade diversification by expanding the available morphological space into which organisms can evolve.

TABLE OF CONTENTS

TABLE OF CONTENTS

ACKNOWLEDGEMENTS

This dissertation would have been impossible for me without the help of many others. UW Biology has been a wonderful place to learn how to become a professional scientist, and I have not once regretted my decision to attend. I would like to particularly thank the many people who helped me tackle the thornier administrative issues (most notably, Sarah O'Hara, Brianna Devine, and Eddie Sabiniano). The department has also been home to extraordinarily helpful research technical staff, especially Wei Pang Chan and Leslie Zeman, who taught me microscopy and histology, which ended up being crucial to the research presented here. Because of my time in UW Biology, I have become a much better teacher, and for this I especially thank Mary Pat Wenderoth, Scott Freeman, Ben Wiggins, Liz Warfield, and Tom Daniel.

I also had the support of many other institutions. Most prominently, Nancy Simmons of the American Museum of Natural History (AMNH) encouraged this project from the very beginning. The AMNH and many other museums provided access to specimens necessary to complete this work: these museums include the Smithsonian National Museum of Natural History, the Museum of Vertebrate Zoology at the University of California Berkeley, the Field Museum, the Slater Museum of Natural History at the University of Puget Sound, and the Texas A&M Research and Teaching Collections. The Lubee Bat Conservancy and Sue Herring also provided fruit bat specimens. Karen Sears of UCLA and her entire lab (Alexa Sadier, Dan Urban, Jen Maier, Neal Anthwal, and Jackie Piekos) were excellent field partners, and they helped me consider developmental implications of my research. The North American Society for Bat Research and the American Society of Mammalogists have been immensely supportive, and I will always recommend that graduate students become active members and attend meetings.

Sharon Swartz and David Boerma of Brown University were crucial to helping me design an experiment to begin to address the complex problem of calcar function. Other members and associates of Sharon's lab (Andrea Rummel, Erika Tavares, Isabel Young, Sascha Morris, and Kenny Breuer) made my visit to Brown both enjoyable and enlightening. Their mix of lab and field experiments has expanded my view of what is possible in studying organismal function.

Each of my committee members (Sue Herring, Adam Summers, Tom Daniel, Dwayne Arola, Greg Wilson) has been instrumental in guiding my research and providing career advice. Greg invited me to interview at UW, and I am very grateful for that opportunity. He also gave me my first field work experience (albeit with fossils!) and helped me recognize the broader evolutionary implications of my studies. Adam's CT scanner has of course been essential, but his excitement for vertebrate biology and interest in student research has been even more valuable and inspiring. Presenting in Sue's lab meetings was essential for rigorously grappling with calcar anatomy, and I am grateful to the entire group for their thoughtful, detailed advice. Sue has helped me understand the complexities of bone growth and development, which has greatly influenced my ideas of skeletal biology and evolution in general. Dwayne consistently gave me the wise advice to not forget my engineering background, and because of this I think I will be a more interdisciplinary scientist. Tom has helped with just about every aspect of being a professional scientist, including teaching (many quarters of Biomechanics!) and research. His influence has inspired me to become an active, giving member of the scientific community, and he also demonstrates that a professor can be both a great scientist and a great teacher.

I would not have been as successful without the help of the Santana Lab. Leith Leiser-Miller, Rochelle Kelly, Abby Vander Linden (and Stephanie Smith!) taught me how to be a member of a biology lab. They also taught me much of what I learned in my first few years about

bats and morphology. Steph also was my partner on our ill-fated 2018 search for the shrew *Sorex merriami*. I was very happy when David Villalobos-Chaves joined the lab so we could add more non-bat (or not entirely bat) diversity to the mix! Ada Kaliszewska and Abbie Curtis often provided me with a sense of perspective as well as much advice on my work, and Jessica Arbour taught me almost everything I know about macroevolutionary modeling (and many other things!). It has been particularly wonderful being a member of Burke Mammalogy. Jeff Bradley has consistently provided patient and enthusiastic and help with whatever I needed, especially with mammal fieldwork and museum prep. He is the best mammal collections manager I know.

I have been extraordinarily lucky to have Sharlene Santana as my dissertation advisor. She encouraged me to fully explore mammal diversity and gave me the freedom to explore my own interests in mammalian morphological evolution, all while consistently providing me with support and advice. She always listened when I burst into her office with a new idea, and I greatly value the time I have had to discuss evolution with her. All of the collaborations mentioned previously were largely due to her proactively introducing me to her colleagues. I look forward to future products of the Santana Lab, which I am sure will be novel and exciting.

Finally, my family. My dad, Richard Stanchak, helped me to be constantly curious about learning new things. My mom, Lisa Trnian, *always* supported me, no matter what, and I would not have received any of my education without her. She also has learned a lot about bats! And Eric Gilbertson helped me understand (1) that science is not as difficult as mountaineering and (2) that I'll be happier if I come home for dinner every night. I bet he never thought he'd know as much about bat feet as he does now.

INTRODUCTION

The Problem of Evolutionary Novelty

The idea of "evolutionary novelty" elicits as many definitions from evolutionary biologists as it does data-driven research. There have been numerous disagreements on what constitutes "novelty" or "*a* novelty" (see Moczek, 2008; Pigliucci, 2008; Wagner, 2014). A major difficulty is that, colloquially, evolutionary novelty is often obvious. For instance, feathers in theropod dinosaurs are a novel morphology, in that they appear in descendants in a clade but not in ancestors. Similarly, tool use is a novel behavior in primates and corvid birds. The reduction in the number of limb bones of horses might also be colloquially termed a novelty, as might the spots on butterfly wings. While it is easy to list novelties, it has been much more difficult to devise a concise and widely agreed upon definition that unites them.

Why have so many evolutionary biologists tried to grapple with such a tenuously-defined term? One reason might be that it is plainly evident to any observer of nature that novelty—however defined—must play a key role in organismal evolution, and thus arduous attempts to expose that role are justified. Unfortunately, theoretical discussions of novelty can quickly devolve into semantic arguments with few real implications for constructive research programs. Data-driven approaches, however, have been very useful in deepening our understanding of novel morphologies and behaviors and what impact they may have on organismal evolution. Perhaps the most notable and relatively recent example is the concept of "deep homology" that grew out of numerous long-term evolutionary-developmental studies of novelty across many animal taxa (Shubin et al., 2009).

In this dissertation, my goal is to take a data-driven approach to the study of evolutionary novelty through a focused study of a novel skeletal element found in bat hindlimbs. The *prima*

facie, informal concepts surrounding novelty provide a starting point for this data-driven, scientific research project:

(1) a novelty is a feature present in a clade that is not found in its ancestors; and

(2) a consequential novelty has had some impact on the evolution of the clade.

Despite their ambiguity, these vague ideas approximate testable hypotheses. Using anatomical, macroevolutionary, and experimental approaches, this dissertation seeks to better understand how novel anatomical features become a functional part of an organism and subsequently diversify, perhaps enabling the diversification of the clade.

The Bat Calcar

Morphological novelty and diversity are ubiquitous throughout Chiroptera. Bats have radiated to fill numerous ecological niches, and they demonstrate corresponding morphological variation. For instance, bats have a highly-modified postcranial skeleton and a series of membranes (patagia) that enable flight. The hindlimb skeleton contains at least one neomorphic feature, the calcar, which articulates with the calcaneus tarsal and extends into the caudal-most membrane, the uropatagium. In a broad comparative review, Schutt and Simmons (1998) demonstrated that the uropatagium, the calcar, and associated musculature vary extensively among bat species. This suggests that these novel structures might have evolved to meet different ecological and functional demands.

Few studies have addressed bat hindlimbs from the perspectives of morphological novelty and functional adaptation; of those that have, most examined a limited number of species or made only qualitative comparisons. Research examining bat hindlimb variation in an

evolutionary context with a current bat phylogeny is especially lacking. This dissertation helps fill both of these knowledge gaps with detailed studies of calcar evolution.

"Additive" Morphological Novelty in the Mammalian Autopod

The tetrapod limb has three levels of organization: the stylopod (humerus/femur), zeugopod (ulna-radius/tibia-fibula), and autopod (wrist/ankle and digits). Skeletal reduction within the autopod is much more common in tetrapods than skeletal addition (Shubin et al., 1997). Tabin (1992) noted that the condition of polydactyly is digit repetition; that is, the 5-digit genetic patterning persists. Shubin et al. (1997) built on this hypothesis and suggested that modifying carpals or tarsals is easier than creating a new digit, as in the case of the radial sesamoid that becomes the "panda's thumb." Mitgutsch et al. (2011) consider a similar problem in the digit-like radial sesamoid of fossorial talpid moles.

Notably, these modified additional autopodial elements in the giant panda and talpid moles enable access to new ecological niches. In the case of the panda's thumb, this arguably led to an evolutionary "dead-end," in which hyper-specialization restricted the diversification of pandas. The mole's thumb, however, may have enabled the modest diversification of talpids as they invaded the fossorial ecospace. In either case, the modified, additional tarsal impacted the evolution of the organismal clade.

While the bat calcar is not exactly digit-like, it is both clearly an element of the autopod yet not a simple modification or repetition of an existing autopodial element. Which, if any, bony or cartilaginous structure it might originate from is unclear, as all bat tarsals have obvious mammalian homologs. In a review on sesamoids and ossicles, Vickaryous and Olson (2007)

consider the calcar and similar membrane support rods in other vertebrate lineages to be "problematic" with regard to their developmental origin.

As a rare skeletal addition, the calcar is especially fascinating because it differs from other autopodial modifications in two important ways: it is widespread at an ordinal level and exhibits extensive interspecific variation. This variation suggests that the calcar is a novel element that has evolved to meet different functional requirements in different bat species. In this dissertation, I capitalize on the systematic diversity of bats and the morphological diversity of bat calcars to illuminate how novelty might influence evolution.

Overview of Dissertation

Chapter 1 – Assessment of the hindlimb membrane musculature of bats: implications for active control of the calcar

In the first chapter, I conduct an anatomical study of the musculature associated with the calcar in three systematically and ecologically distinct bat species (with co-author Sharlene Santana). We found that the arrangement of calcar musculature varies among the three species, such that bats with higher maneuverability requirements in flight (i.e., aerial insectivores) exhibit more complex calcar and calcar musculature morphologies than the species with lower maneuverability requirements (i.e., a frugivore that feeds on stationary food items). This chapter serves as a detailed introduction to calcar and uropatagium anatomy, and its findings are suggestive of ecologically-relevant anatomical variation that informs Chapters 2 and 3.

***Chapter 2* – Anatomical diversification of a skeletal novelty in bat feet**

The second chapter has two goals: to broadly compare calcar skeletal anatomy across Chiroptera and to test an early burst model of calcar morphological diversification. (Co-authors are Jessica Arbour and Sharlene Santana). We find that the calcar varies extensively among bats in length and skeletal tissue composition, and that in many species it articulates with the calcaneus ankle bone at a synovial joint. Comparisons of evolutionary models of calcar length and corresponding disparity-through-time analyses indicate that the calcar diversified early in bat evolutionary history as they phylogenetically diversified after evolving the capacity for flight.

***Chapter 3* – Motion of the calcar during fight in *Carollia perspicillata* (Phyllostomidae: Chiroptera)**

The third chapter seeks to improve our understanding of calcar function by exploring two basic questions – does the calcar move in flight, and if so, how? My findings about calcar anatomy (Chapters 1 and 2), specifically the presence of a synovial joint, suggest the calcar is capable of moving about its joint with the calcaneus. To measure calcar motion, I collected high-speed video recordings of *Carollia perspicillata* individuals in a relatively-controlled laboratory setting and tracked the rotation of the tip of the calcar about other hindlimb elements. We found that the calcar does rotate about its joint in steady-forward flight in *C. perspicillata*, and that rotation in the approximately dorsal-ventral plane is greater than rotation in the approximately anterior-posterior plane. (Conducted in collaboration with David Boerma, Sharlene Santana, and Sharon Swartz, in preparation for publication.)

Each chapter consists of an abstract followed by complete introduction, methods, results, and discussion sections and can be read in isolation of the other two. Figures and tables referenced in the main text of each chapter can be found just prior to that chapter's references. Supporting Information for each chapter can be found just after that chapter's references. Large data files have been submitted as supporting electronic files with the dissertation.

All three chapters together provide the most complete scientific exploration of the calcar to-date. They are followed by a conclusion that (1) considers the implications of this dissertation for the general study of evolutionary novelty and (2) outlines a promising future research program centered on the bat calcar to further our understanding of morphological evolution, skeletal biology, and animal flight.

REFERENCES

Mitgutsch, C, MK Richardson, R Jiménez, JE Martin, P Kondrashov, MAG de Bakker, MR Sánchez-Villagra. (2011) Circumventing the polydactyly 'constraint': the mole's 'thumb' Biology Letters DOI:10.1098/rsbl.2011.0494.

Moczek, A.P. 2008. On the origins of novelty in development and evolution. BioEssays 30:432-447.

Pigliucci, M. 2008. What, if anything, is an evolutionary novelty? Philos. Sci. 75:887-898.

Schutt, W.A., and N.B. Simmons. 1998. Morphology and homology of the chiropteran calcar, with comments on the phylogenetic relationships of Archaeopteropus. J. Mamm. Evol. 5:1-32.

Shubin N, C Tabin, S Carroll. (1997) Fossils, genes and the evolution of animal limbs. Nature 388:639-648.

Shubin, N., Tabin, C., and S. Carroll. 2009. Deep homology and the origins of evolutionary novelty. Nature 457:818-823.

Tabin CJ. (1992) Why we have (only) five fingers perhand: Hox genes and the evolution of paired limbs. Development 116:289-296.

Vickaryous, M.K., and W.M. Olson. 2007. Sesamoids and ossicles in the appendicular skeleton. *Fins into limbs: evolution, development and transformation*. Univ. Chicago Press.

Wagner, G.P. 2014. *Homology, genes, and evolutionary innovation*. Princeton Univ. Press.

CHAPTER 1

Assessment of the Hindlimb Membrane Musculature of Bats: Implications for Active Control of the Calcar

Authors:

Kathryn E. Stanchak [1] *, Sharlene E. Santana [1]

[1]Department of Biology and Burke Museum of Natural History and Culture, University of Washington, Seattle, Washington 98195, USA

A version of this manuscript was published in *The Anatomical Record*:

Stanchak, K. E., and Santana, S. E. (2018). Assessment of the hindlimb membrane musculature of bats: implications for active control of the calcar. *The Anatomical Record*, 301(3), 441-448.

ABSTRACT

The striking postcranial anatomy of bats reflects their specialized ecology; they are the only mammals capable of powered flight. Bat postcranial adaptations include a series of membranes that connect highly-modified, or even novel, skeletal elements. While most studies of bat postcranial anatomy have focused on their wings, bat hindlimbs also contain many derived and functionally important, yet less studied, features. In this study, we investigate variation in the membrane and limb musculature associated with the calcar, a neomorphic skeletal structure found in the hindlimbs of most bats. We use diffusible iodine-based contrast-enhanced computed tomography and standard histological techniques to examine the calcars and hindlimb membranes of three bat species that vary ecologically (*Myotis californicus*, a slow-flying insectivore; *Molossus molossus*, a fast-flying insectivore; and *Artibeus jamaicensis*, a slow-flying frugivore). We also assess the level of mineralization of the calcar at muscle attachment sites to better understand how muscle contraction may enable calcar function. We found that the arrangement of the calcar musculature varies among the three bat species, as does the pattern of mineral content within the calcar. *M. molossus* and *M. californicus* exhibit more complex calcar and calcar musculature morphologies than *A. jamaicensis*, and the degree of calcar mineralization decreases towards the tip of the calcar in all species. These results are consistent with the idea that the calcar may have a functional role in flight maneuverability.

INTRODUCTION

The evolution of flight and associated morphologies in bats (Chiroptera) is an example of how anatomical evolution can enable new functional abilities and lead to ecological diversification (Teeling et al., 2005; Simmons, 2005). Once bats evolved a highly-modified postcranial skeleton and a series of membranes (patagia) that enabled powered flight (Fig. 1), they radiated to fill numerous ecological niches and evolved corresponding morphological and functional specializations (Norberg and Rayner, 1987). For instance, the shape of wing membranes varies among bats, corresponding with different flight ecologies among species (Norberg and Rayner, 1987). Furthermore, bat membranes contain musculature, associated nerves, and elastin fibers that vary across species, and are hypothesized to contribute to the mechanical properties of the membrane and to both active and passive control of membrane shape during flight (Holbrook and Odlund, 1978; Swartz et al., 1996; Cheney et al., 2014a; Cheney et al., 2017).

Postcranial studies of bats have primarily focused on the forewing (e.g., wing membranes: Cheney et al., 2014a and 2017; wing bones: Swartz et al. 1992; forelimb development: Sears et al. 2006). However, bat hindlimbs are also highly modified and presumably specialized for many tasks, including prey capture and hanging, as well as flight (Fish et al, 1991; Simmons and Quinn, 1994; Cheney et al., 2014b). Because bats are ecologically diverse, the functional requirements of these tasks vary widely among species. As such, the primary evolutionary pressures on hindlimb morphology likely differ among species, leading to functionally-relevant variation. Supporting this idea, the shape and size of the uropatagium vary considerably among bat species (Hill and Smith, 1984; Schutt and Simmons, 1998). Furthermore, bats have evolved a calcar, a neomorphic (Hall, 1995) spur of cartilage that

arises from the bat ankle, articulates with the calcaneus tarsal, and extends into the posterior margin of the uropatagium (Fig. 1). The calcar suddenly appears in the oldest known bat postcrania (*Onychonycteris finneyi*, ca. 52.5 Ma, Simmons et al., 2008) and is found in a large majority of bat species, although it has been lost in some (Schutt and Simmons, 1998). Analogous but not homologous structures are known from other tetrapod lineages, including the styliform cartilages of gliding rodents, the pteroid of pterosaurs, and the styliform element of the membrane-bound maniraptor *Yi qi* (Xu et al., 2015). Because the calcar is found throughout a speciose and diverse clade (Chiroptera), it provides a unique opportunity to study morphological and functional diversity in newly-evolved skeletal elements.

Little is known about the function of the calcar and its associated musculature, as there are few detailed anatomical studies of these structures. Schutt and Simmons (1998) presented a broad overview of the calcar and associated musculature across all bat families. These descriptions built upon previous work by Humphry (1869), MacAlister (1872), Maissonneuve (1878), Morra (1899), de Fénis (1919), Vaughan (1959, 1970a), Mori (1961), and Grassé (1971). (For a full review, see Schutt and Simmons, 1998). In all bats that had a calcar, they found two muscles that attach to the calcar: the *m. calcaneocutaneous* and the *m. depressor ossis styliformis*. They depicted the *m. calcaneocutaneous* as originating from the anterior margin of the calcar and inserting onto the medial raphe of the uropatagium posterior to the tail. As tail length varies among bat species, often extending to the posterior margin of the uropatagium, the insertion of the *m. calcaneocutaneous* is variable. The *m. depressor ossis styliformis* originates from the fifth metatarsal and the medial surface of the calcaneus and inserts onto the posterior margin of the calcar. Schutt and Simmons (1998) also noted that the calcar is present in both mineralized and unmineralized forms in different species of bats, and they suggested that

variation in calcar and uropatagium shape, size, and structure has implications for dietary and foraging strategies.

In the present study, our goal is to better understand the anatomy of the uropatagial musculature associated with the calcar, its variation among species, and its possible function. We expand upon previous descriptions of bat uropatagial anatomy by detailing interspecific differences in the musculature that controls the calcar among three distantly-related bat species that vary morphologically and ecologically: (1) *Myotis californicus* (Vespertilionidae), an aerial insectivore with relatively slow flight; (2) *Molossus molossus* (Molossidae), an aerial insectivore with fast flight; and (3) *Artibeus jamaicensis* (Phyllostomidae), a frugivore that forages within the cluttered forest (Norberg and Rayner, 1987). Aerial insectivores like *M. californicus* capture small, agile prey during flight and thus must be able to change directions quickly. Molossid bats like *M. molossus* are also aerial insectivores, but they are morphologically adapted to reduce drag and fly fast over long distances and are consequently less maneuverable over short distances (Vaughan, 1970b). Both of these species use their uropatagium to aid in prey capture. Conversely, frugivores capture and feed on stationary targets; *A. jamaicensis* grabs fruits with its mouth and consumes them while hanging (rather than consuming the fruits while hovering like nectarivorous bats). Due to these differences in requirements for maneuverable flight, it has been suggested that frugivores possess a less specialized flight apparatus (Vaughan, 1970b). Here, we test the hypothesis that the morphology of the calcar and associated musculature will vary among *M. californicus*, *M. molossus*, and *A. jamaicensis* due to the different functional requirements of their flight patterns. We expect that species that require higher flight maneuverability and/or flight speeds (aerial insectivores) will exhibit a more complex calcar muscle arrangement that

allows for finer control of calcar motion, whereas the less maneuverable frugivore will exhibit a simpler calcar muscle arrangement.

MATERIALS AND METHODS

DiceCT and Virtual Dissections

We used diffusible iodine-based contrast-enhanced computed tomography (diceCT; Gignac et al. 2016) to assess calcar musculature anatomy, as this method allowed us to study the morphology of soft tissue elements without causing permanent damage to the original specimens. We dissected one hindlimb from one specimen each of *M. californicus, M. molossus*, and *A. jamaicensis*. These specimens had previously been preserved in 10% neutral-buffered formalin (NBF) and then stored in 70% ethanol. We placed each hindlimb into a 3% w/v Lugol's iodine solution (1% w/v I_2, 2% w/v KI). Because the bats varied in size, they required different staining times in the iodine solution: *M. californicus*, 2 days; *M. molossus*, 3 days; *A. jamaicensis*, 4 days. We scanned each specimen in a Skyscan 1172 µCT scanner (Bruker MicroCT, Belgium) at 40 kV and 201 µA with a 0.5 mm aluminum filter at a resolution of 11.76 µm. We also scanned a separate iodine-stained specimen of *M. californicus* at a higher resolution (6.34 µm) to better distinguish features during the virtual dissection. To ensure that the uropatagia remained in an extended position during the scan, we sewed each hindlimb with the membrane extended to a piece of styrofoam. We reconstructed our X-ray projections from the µCT scans using NRecon software (Bruker MicroCT, Belgium) and viewed our reconstructed scans using CTvox (Bruker MicroCT, Belgium), a volume-rendering software that allows for 3D visualization of CT scans. We used DataViewer (Bruker MicroCT, Belgium) to measure the length of the tibia of each bat as a scale for the CTvox images. We then imported our

reconstructed scans into Mimics 18.0 (Materialize, Ann Arbor, MI, USA) and digitally dissected the calcar, the *m. depressor ossis styliformis*, and adjacent anatomical features. We also used Mimics 18.0 to measure the total calcar length of each specimen.

Conventional CT Scanning and Mineralization Observations

To better assess the functional implications of variation in calcar musculature anatomy and to support our diceCT results, we also μCT scanned one hindlimb from different specimens of each of the target species (Skyscan 1172; 50-60 kV and 167-201 μA with a 0.5 mm aluminum filter). To evaluate calcar mineralization, we scanned these specimens with 0.25 and 0.75 calcium hydroxyapatite (CaHA) standards (Bruker MicroCT, Belgium). The specimens used had been fixed in 10% NBF for variable periods of time prior to storage in 70% ethanol. Because formalin is a mild decalcifier, any quantitative results based on this method are inaccurate; rather, our intent was to use both the diceCT and conventional CT scans to qualitatively assess mineral content within each scan to determine which portions of the calcar were calcified or uncalcified.

Histology

After diceCT scanning, we leached the iodine from the hindlimbs by placing them in several washes of 70% ethanol over the course of one week. To speed the leaching process, we placed the specimens in their leaching solution in a 37ºC shaker. We then dissected the hindlimbs into uropatagium and calcar/depressor muscle pieces. With the help of the volume-rendered CTvox images, we attempted to dissect these pieces such that we could obtain cross-sections of the *m. depressor ossis styliformis* perpendicular to the longitudinal plane of the

calcar, and sections of the *m. calcaneocutaneous* in the plane perpendicular to the muscle fiber orientation. We placed all mineralized pieces of tissue (*M. molossus* and *M. californicus* calcars) in a 12% EDTA solution in a 37ºC shaker for one week to decalcify. To prepare for histological sectioning, we dehydrated all tissue pieces through a series of increasing ethanol concentrations, cleared them in xylene, and infiltrated them with paraffin wax. We then embedded each piece in a paraffin block, cut the block into 6 μm sections on a Leica RM2145 microtome, and cleared and rehydrated each section. We stained the sections with Modified Mayer's Hematoxylin followed by a Mallory triple connective tissue stain (Humason, 1962). We briefly soaked each section in 1% acetic acid before dehydrating them through the alcohol series, clearing them with xylene, and mounting them with a xylene-toluene resin and coverslip. We imaged the sections with a Nikon Eclipse E600FN compound microscope and an AmScope MU300 microscope-mounted camera.

RESULTS

Gross Anatomy of Calcar Musculature

Myotis californicus – The uropatagial muscles are composed of distinct, separate bundles of fibers (Fig. 2a). The CTvox rendering of the diceCT scan appears to show one bundle near the ankle joint originating from the calcar itself (the *m. calcaneocutaneous*), although small folds in the membrane made this difficult to discern. The remainder of the bundles originates from the tibia, forming the *m. tibiocutaneous*. We did not see attachment of the *m. calcaneocutaneous* to the calcar in any histological sections. Virtual dissection from the diceCT scan revealed that the *m. depressor ossis styliformis* of *M. californicus* originates from both the calcaneus and the cuboid and inserts onto the posterior margin of the calcar (Fig. 3a). The diceCT scan also

revealed an uncalcified spur on the posterior margin of the calcar, onto which the medial edge of the *m. depressor ossis styliformis* appears to insert (Figs. 3a and 4a).

Molossus molossus – The *m. calcaneocutaneous* is a flat sheet of fibers along the dorsal side of the uropatagium that originates from the anterior margin of the calcar. These are not immediately recognizable in the CTvox rendering of the diceCT scan, but they are visible in histological sections (Fig. 2b and Fig. 4c,d). The *m. depressor ossis styliformis* consists of two separate muscle compartments. The first, which we call the *m. depressor ossis styliformis profundus*, originates from the calcaneus and inserts onto the portion of the calcar proximal to the ankle, wrapping around the posterior margin. The second, the *m. depressor ossis styliformis superficialis*, originates from the 5th metatarsal, runs beneath the *m. depressor ossis styliformis profundus* and inserts distally along the calcar, closer to the tail and the midline of the uropatagium (Figs. 3b and 4b). We also noticed an additional muscle that runs beneath the *m. depressor ossis styliformis* (Fig. 4c). This additional muscle extends medially to a sheath of muscle surrounding the tail, but its origination and insertion are unclear from the diceCT scans. It was not found in the other two species.

Artibeus jamaicensis – Of the three bats examined, the calcar musculature of *A. jamaicensis* best conforms to previous descriptions (Schutt and Simmons, 1998). The *m. calcaneocutaneous* is a relatively thick, flat sheet of regularly-arranged fibers originating from the anterior margin of the calcar (Figs. 2c and 4b). The *m. depressor ossis styliformis* originates from the fifth metatarsal and inserts onto the posterior margin of the calcar (Figs. 3c and 4d). The calcar of *A. jamaicensis* is relatively shorter than those of the other two bats, and the *m. depressor ossis styliformis* runs almost the entire length of the calcar, rather than only inserting on the half proximal to the ankle.

Calcar Length and Mineralization

Both the conventional CT and the diceCT scans revealed notable differences in calcar length among the three bat species (see CTvox renderings of diceCT scans in Fig. 2). In *M. californicus*, the calcar spans approximately 50% of the distance between the ankle and the tail (13.6 mm), leaving the posterior edge of the uropatagium closest to the tail unsupported. In *M. molossus*, the calcar tapers to a thin band approximately 70% of the distance between the ankle and the tail (12.9 mm). We were unable to follow the full length of this band in the diceCT scan to determine if it is connected to the tail or the sheath of muscle surrounding the tail. In *A. jamaicensis*, the calcar extends to the medial edge of the uropatagium and is relatively shorter than those of the other two bats examined (3.2 mm), possibly because this species has a reduced uropatagium (Fig. 2c).

Both the conventional and the diceCT scans of iodine-stained bat hindlimbs showed variable pixel intensity within the calcar of each individual bat, indicating variation in mineralization along the length of the calcar. The calcars of *M. californicus* and *M. molossus*, in particular, are more mineralized near the ankle and unmineralized closer to the tail (Fig. 3). In both of these species, the length of the mineralized portion corresponds with the insertions of the *m. depressor ossis styliformis*. The calcar of *A. jamaicensis* exhibits a small, calcified nodule near the joint with the calcaneus, but is largely unmineralized, even along the insertion of the *m. depressor ossis styliformis*.

DISCUSSION

Functional Implications of Interspecific Variation in Uropatagium and Calcar Musculature

The hindlimb membrane apparatus of bats underwent great morphological diversification as the lineage radiated to fill different ecological niches. The presence of muscles that originate from and insert onto the calcar and the observed variation in the arrangement of these muscles among species likely reflect functional aspects of ecological diversification. Our results suggest that bats vary in the amount of control they have over the motion of the calcar and thus, the shape of the uropatagium, and that this variation may correspond with different flight ecologies.

The presence of two distinct depressor muscles that insert onto the calcar of *M. molossus* is a remarkable finding that indicates that this bat has independent control over the portion of the calcar closer to the ankle and the portion more distal from the ankle. This would give *M. molossus* fine control over the expansion and shape of the uropatagium. In contrast, *A. jamaicensis* and *M. californicus* have only one muscle that depresses the calcar. The *m. depressor ossis styliformis* of *M. californicus*, however, inserts onto both the main body of the calcar and onto a cartilaginous spur of the calcar that projects into the posterior margin of the uropatagium. Consequently, a contraction of the *m. depressor ossis styliformis* in *M. californicus* would serve to spread the uropatagium in posterior and lateral directions simultaneously. Thus, the presence of two distinct depressor muscles in *M. molossus* and a cartilaginous calcar spur in *M. californicus* may be two different solutions to enhance control of the uropatagium as these species pursue and capture fast insect prey. While maneuverability is also important for *A. jamaicensis* as it navigates cluttered forest habitat, the agility required to avoid tree branches and locate fruits may present less of a functional challenge than that required to catch flying insects (Vaughan, 1970b). Flight agility and maneuverability have been experimentally compared

between insectivorous species of bats (Aldridge, 1986 and Aldridge et al., 1987) and between frugivores (Stockwell, 2001), but additional studies comparing the same agility and maneuverability patterns among bats of different ecologies and with different flight patterns are required to further support this idea.

The *m. calcaneocutaneous* also varies among the three bat species we examined. First, the fibers of the sheet-like *m. calcaneocutaneous* are more sparsely distributed in *M. molossus* than in *A. jamaicensis*. *M. molossus* has a unique sheath of muscle surrounding its tail vertebrae. This muscle might actuate the retraction of the uropatagium along the tail either to free the hindlimbs as the bat moves quadrupedally in crevices or to reduce drag during flight (Vaughan, 1966). Thus, the *m. calcaneocutaneous* may play less of a role in controlling the uropatagium than the tail sheath in *M. molossus*. It is also possible that the elastic properties of the muscle fibers of the *m. calcaneocutaneous* serve to passively counter the action of the *m. depressor ossis styliformis* in either of these species, for example by tightening the membrane to reduce flutter during flight. Second, most if not all of the membrane muscle bundles in *M. californicus* form the *m. tibiocutaneous* (Schutt and Simmons, 1998) rather than the *m. calaneocutaneous*. This suggests that *M. californicus* has limited control of its calcar from producing anterior (elevator) forces. Even if one or more muscle bundles do originate from the ankle joint, the total cross-sectional area of the muscle would be quite small, and any force produced would be near the pivot point of the joint, generating little torque. This indicates that there is no or very little antagonistic torque to counter the *m. depressor ossis styliformis* in *M. californicus*.

Calcar Length, Mineralization, and Muscle Attachments

The length of the calcar, and the extent to which it spans and supports the posterior margin of the uropatagium, varies considerably among the three species studied. In *M. californicus*, the edge of the uropatagium closest to the tail is unsupported by the calcar, resulting in a trailing edge that is free to flutter unless stretched by the surrounding skeleton and musculature. The calcar of *M. molossus* also does not extend fully to the tail, but the additional, undescribed muscle we found may provide some stiffness to the posterior margin of the uropatagium closest to the tail.

Our CT scans revealed variation in mineral content along individual calcars, which indicates that material properties also vary along calcars. This has implications for the response of the calcar to the force produced by the contractions of the muscles that insert onto it. A contraction of the *m. inferior ossis styliformis* may cause an uncalcified or little-calcified calcar to bend rather than (or as well as) rotate about its articulation with the calcaneus. This additional source of calcar variation might give bats finer control over the extent to which their uropatagium is spread, thus helping them change the amount of lift produced and drag experienced during flight.

Future Work and Conclusions

Our anatomical findings have led to several hypotheses about the function and physiology of the uropatagium and calcar muscles. To test these, future work should examine the innervation of these muscles, as well as test biomechanical models of the calcar apparatus. Tokita et al. (2012) used a developmental approach to study the innervation of wing membrane muscles in two vespertilionid species. They discovered that the *m. calcaneocutaneous* (called the

m. uropataginalis in their study) is primarily innervated by a branch of the lumbar and sacral plexuses that corresponds to a branch innervating the semitendinosus. However, they did not provide detailed information on the innervation of each bundle of fibers nor on the innervation of the *m. depressor ossis styliformis*. Our results indicate that it is particularly important to determine the innervation of the depressor muscle complex in *M. molossus* to test our hypothesis that the *m. depressors ossis styliformis profundus* and *superficialis* can contract independently.

We have presented only qualitative descriptions of the muscles associated with the calcar and of calcar mineral content to explore functional variation of the calcar apparatus. To fully understand the implications of calcar anatomical variation to flight performance, future research should build proper quantitative biomechanical models that account for the force of muscle contraction and the bending resistance of the calcar (including measurements of elastic moduli and cross-sectional shape). As the bat calcar is a neomorphic structure that takes on diverse anatomical configurations among bats species, these kinds of studies may serve to improve our understanding of morphological novelty and diversification in the vertebrate skeleton.

ACKNOWLEDGEMENTS

We greatly appreciate the donation of *Myotis californicus* specimens from the Washington State Department of Health and *Molossus molossus* specimens from the Slater Museum of Natural History to the Burke Museum of Natural History and Culture. J.H. Arbour, A.A. Curtis, Z.A. Kaliszewska, L.B. Miller, and two anonymous reviewers provided useful comments that helped us greatly improve the manuscript. The Iuvo Award from the University of Washington Department of Biology provided K.E. Stanchak with funding for histological supplies.

FIGURES

Figure 1. Extended wing of *Myotis* sp. demonstrating the series of patagia that form the bat wing and the location of the calcar.

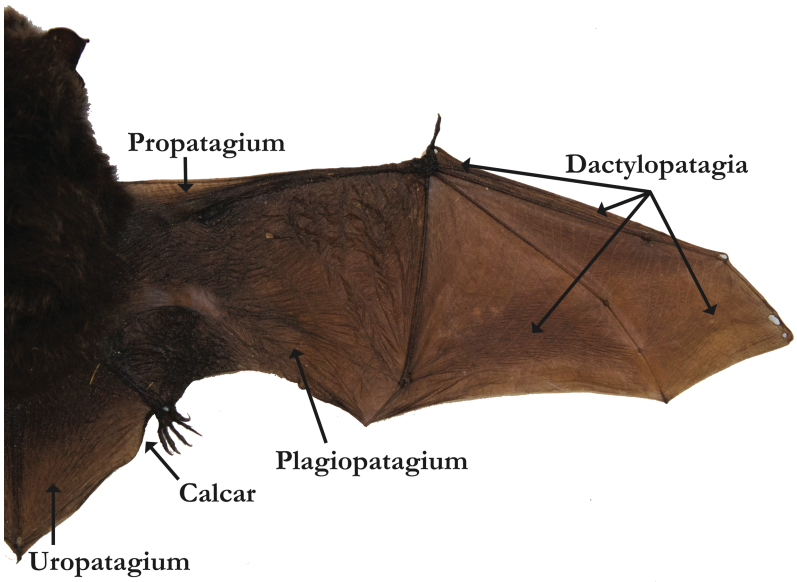

Figure 2. Mallory-stained histological sections through the uropatagia of (a) *Myotis californicus*, (b) *Molossus molossus*, and (c) *Artibeus jamaicensis*. The dorsal side of each section is on the upper half of the image. Arrows point to the uropatagial cutaneous muscles (*m. tibiocutaneous* in a; *m. calcaneocutaneous* in b and c). Scale bars on the histological sections are 100 µm. Insets for each image indicate the approximate location of each section on the volume-rendered diceCT scan of each specimen. For comparing relative size, the tibia lengths for each specimen are (a) 12.4 mm, (b) 14.4 mm, and (c) 19.5 mm.

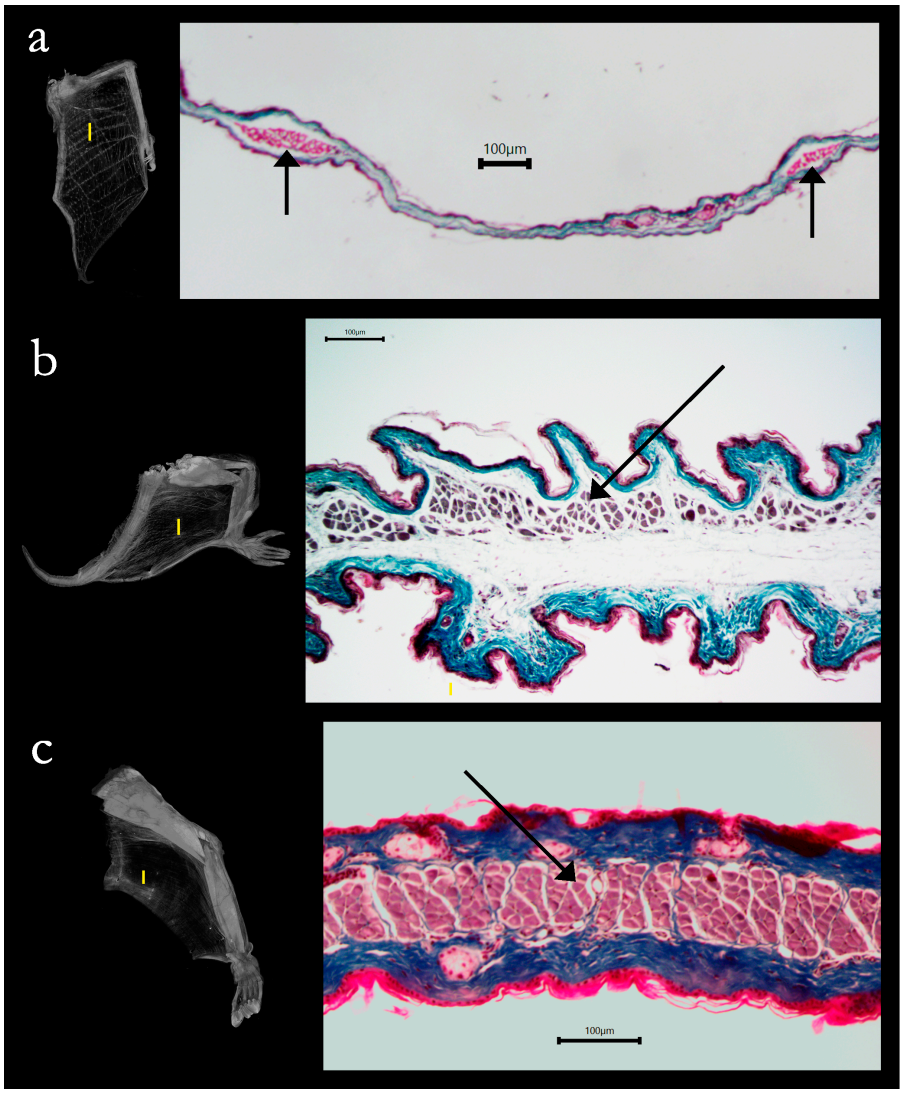

Figure 3. Virtual dissections in ventral view of the calcar-depressor muscle complex of one hindlimb each of (a) *Myotis californicus*, (b) *Molossus molossus*, and (c) *Artibeus jamaicensis*. The inset illustrates the location of the dissection models using the *A. jamaicensis* volume-rendered diceCT scan. The tips of the calcars of *M. californicus* and *M. molossus* are cropped to better view the ankle region. Ca-m, mineralized calcar; Ca-um, unmineralized calcar; Cs, calcaneus; Cu, cuboid; m.D, *m. depressor ossis styliformis*; m.DP, *m. depressor ossis styliformis profundus*; m.DS, *m. depressor ossis styliformis superficialis*; Mt5, fifth metatarsal.

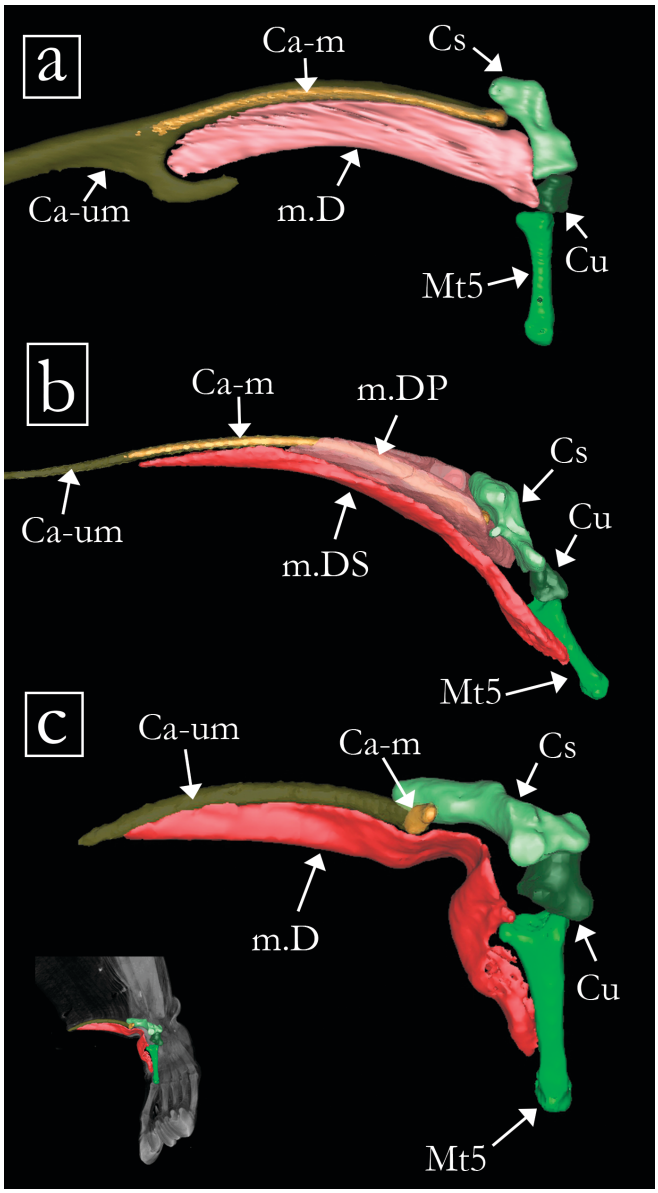

Figure 4. Mallory-stained histological sections through the calcar of (a) *Myotis californicus*, (b) and (c) *Molossus molossus*, and (d) *Artibeus jamaicensis*. The anterior side of each section is on the upper half of the image. Insets for each image indicate the approximate location of each section on the volume-rendered diceCT scan of each specimen. Scale bars are 100 µm. Ca, calcar; m.A, additional muscle in *M. molossus*; m.CC, *m. calcaneocutaneous*; m.D, *m. depressor ossis styliformis*; m. DP, *m. depressor ossis styliformis profundus*; m.DS, *m. depressor ossis styliformis superficialis*.

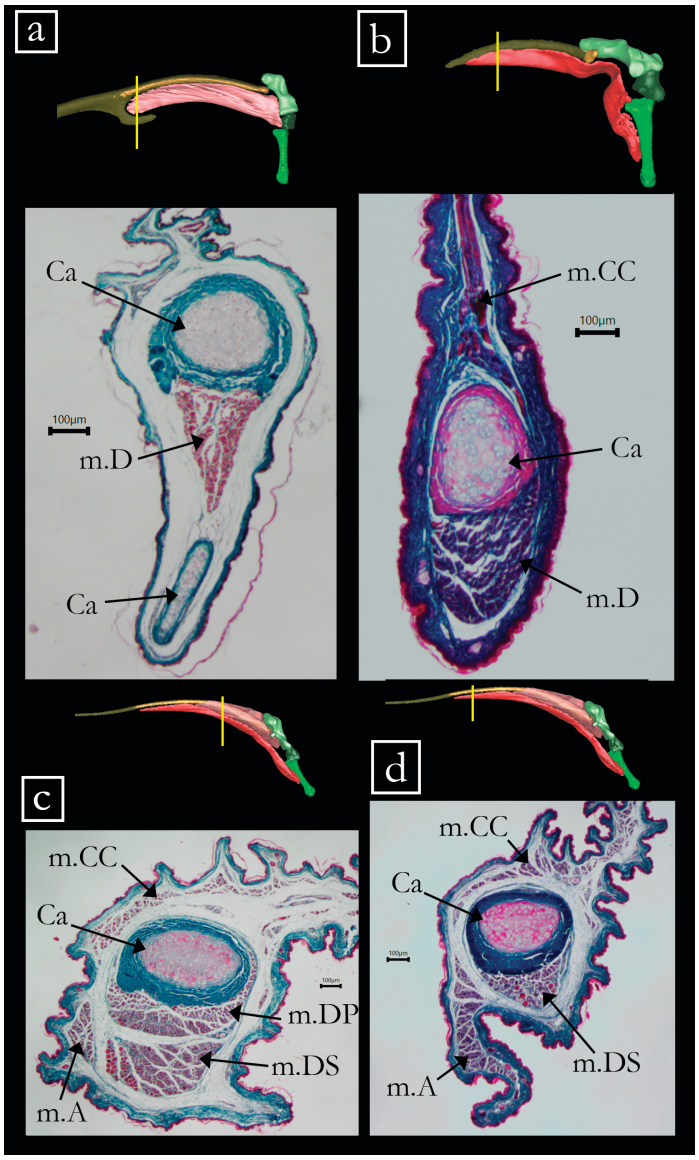

REFERENCES

Aldridge H. 1986. Manoeuvrability and ecological segregation in the little brown (Myotis lucifugus) and Yuma (M. yumanensis) bats (Chiroptera: Vespertilionidae). Canadian J. of Zoo. 64(9):1878-1882.

Aldridge HD, Rautenbach JH, Rautenbach IL. 1987. Morphology, echolocation and resource partitioning in insectivorous bats. J. Animal Ecology. 763-778.

Cheney JA, Konow N, Middleton KM, Breuer KS, Roberts TJ, Giblin EL, Swartz SM. 2014a. Membrane muscle function in the compliant wings of bats. Bioinspir Biomim 9, 025007.

Cheney JA, Ton D, Konow N, Riskin DK, Breuer KS, Swartz SM. 2014b. Hindlimb motion during steady flight of the lesser dog-nosed fruit bat, *Cynopterus brachyotis*. PloS one 9(5):e98093.

Cheney JA, Allen JJ, Swartz S. M. 2017. Diversity in the organization of elastin bundles and intramembranous muscles in bat wings. J Anat 230: 510-523.

de Fénis F. 1919. Le membre pelvien des Chiroptères. Ses caractères d'adaptation a la suspension, Thèses pour obtenir le grade de Docteur des Sciences Naturelles, L'Uinversité de Paris. 823, d'ordre 1619.

Fish FE, Block BR, Clark BD. 1991. Hydrodynamics of the feet of fish-catching bats: influence of the water surface on drag and morphological design. J Exp Zoo 258:164-173.

Gignac PM, Kley NJ, Clarke JA, Colbert MW, Morhardt AC, Cerio D, Cost IN, Cox PG, Daza JD, Early CM, Echols MS, Henkelman RM, Herdina AN, Holliday CM, Li Z, Mahlow K, Merchant S, Müller J, Orsbon CP, Paluh DJ, Thies ML, Tsai HP, Witmer LM. 2016.

Diffusible iodine-based contrast-enhanced computed tomography (diceCT): an emerging tool for rapid, high-resolution, 3-D imaging of metazoan soft tissues. J Anat 228: 889–909.

Grassé PP. 1971. Muscles de la jambe et du pied—Les Chauves-souris. In: Grassé PP, editor. Traité de Zoologie Tome 17. Paris: Maison et Cie. pp 386-391.

Hill JE, Smith JD. 1984. Bats: A Natural History. London: British Museum (Natural History).

Holbrook KA, Odlund GF. 1978. A collagen and elastic network in the wing of the bat. J Anat 126:21-36.

Humason GL. 1962. Animal Tissue Techniques. 2nd ed. San Francisco: W.H. Freeman & Co.

Humphry GM. 1869. The myology of the limbs of Pteropus. J Anat Physiol 3:294-491.

MacAlister A. 1872. The myology of the cheiroptera. Philos Trans R Soc Lond B Biol Sci 162:125-171.

Maisonneuve P. 1878. Traité de l'ostéologie et de la myologie du Vespertilio murinus, précédé d'un exposé de la classification des chéiroptères et de considérations sur les moeurs de ces animaux. Paris: Ed: Doin.

Mori M. 1960. Muskulatur des Pteropus edulis. Okajimas Folia Anat Jpn 36:253-307.

Morra T. 1899. I muscoli cutanei della membrana alare dei chirotteri. Bull Mus Zool Ed Anat Comp R. Univ Di Torino XIV, 1–7.

Norberg UM, Rayner JMV. 1987. Ecological morphology and flight in bats (Mammalia; Chiroptera): wing adaptations, flight performance, foraging strategy and echolocation. Philos Trans R Soc Lond B Biol Sci 316:335-427.

Schutt Jr. WA, Simmons NB. 1998. Morphology and Homology of the Chiropteran Calcar, with Comments on the Phylogenetic Relationships of Archaeopteropus. J Mamm Evol; 5:1-32.

Sears KE, Behringer RR, Rasweiler JJ, Niswander LA. 2006. Development of bat flight: morphologic and molecular evolution of bat wing digits. PNAS 103:6581-6586.

Simmons NB, Quinn TH. 1994. Evolution of the digital tendon-locking mechanism in bats and dermopterans: a phylogenetic perspective. J Mamm Evol 2:213-254.

Simmons NB. 2005. Order Chiroptera, In: Wilson, DE and Reeder DM, editors. Mammal Species of the World: a taxonomic and geographic reference. Baltimore, MD: Johns Hopkins University Press. pp 312-529.

Simmons NB, Seymour KL, Habersetzer J, Gunnell GF. 2008. Primitive Early Eocene bat from Wyoming and the evolution of flight and echolocation. Nature 451:818-821.

Stockwell EF. 2001. Morphology and flight manoveurability in New World leaf-nosed bats (Chiroptera: Phyllostomidae). J. Zoology. 254(4):505-514.

Swartz SM, Bennett MB, Carrier DR. 1992. Wing bone stresses in free flying bats and the evolution of skeletal design for flight. Nature. 359:726-729.

Swartz SM, Groves MS, Kim HD, Walsh WR. 1996. Mechanical properties of bat wing membrane skin. J Zool 239:357-378.

Teeling EC, Springer MS, Madsen O, Bates P, O'brien SJ, Murphy WJ. 2005. A molecular phylogeny for bats illuminates biogeography and the fossil record. Science 307:580-584.

Tokita M, Abe T, Suzuki K. 2012. The developmental basis of bat wing muscle. Nat Comm 3:1302.

Vaughan TA. 1959. Functional morphology of three bats: Eumops, Myotis, Macrotus. University of Kansas Publications, Museum of Natural History 12:1-153.

Vaughan TA. 1966. Morphology and Flight Characteristics of Molossid Bats. J Mamm 47:249-260.

Vaughan TA. 1970a. The muscular system, In: Wimsatt WA, editor. Biology of Bats Vol. 1. New York: Academic Press. pp 139-194.

Vaughan TA. 1970b. Flight patterns and aerodynamics, In: Wimsatt WA, editor. Biology of Bats Vol. 1. New York: Academic Press. pp 195-216.

Xu X, Zheng X, Sullivan C, Wang X, Xing L, Wang Y, Zhang X, O'Connor JK, Zhang F, Pan Y. 2015. A bizarre Jurassic maniraptoran theropod with preserved evidence of membranous wings. Nature 455:1105-1108.

CHAPTER 2

Anatomical diversification of a skeletal novelty in bat feet

Authors:

Kathryn E. Stanchak [1] *, Jessica H. Arbour [1], Sharlene E. Santana [1]

[1]Department of Biology and Burke Museum of Natural History and Culture, University of Washington, Seattle, Washington 98195, USA

A version of this manuscript was published in *Evolution*:

Stanchak, K. E., Arbour, J. H., and Santana, S. E. (2019). Anatomical diversification of a skeletal novelty in bat feet. *Evolution* 73,1591-1603.

ABSTRACT

Neomorphic, membrane-associated skeletal rods are found in disparate vertebrate lineages, but their evolution is poorly understood. Here we show that one of these elements—the calcar of bats (Chiroptera)—is a skeletal novelty that has anatomically diversified. Comparisons of evolutionary models of calcar length and corresponding disparity-through-time analyses indicate that the calcar diversified early in the evolutionary history of Chiroptera, as bats phylogenetically diversified after evolving the capacity for flight. This interspecific variation in calcar length and its relative proportion to tibia and forearm length is of functional relevance to flight-related behaviors. We also find that the calcar varies in its tissue composition among bats, which might affect its response to mechanical loading. We confirm the presence of a synovial joint at the articulation between the calcar and the calcaneus in some species, which suggests the calcar has a kinematic functional role. Collectively, this functionally-relevant variation suggests that adaptive advantages provided by the calcar led to its anatomical diversification. Our results demonstrate that novel skeletal additions can become integrated into vertebrate body plans and subsequently evolve into a variety of forms, potentially impacting clade diversification by expanding the available morphological space into which organisms can evolve.

INTRODUCTION

In *On the Origin of Species*, Darwin repeatedly argued against the abrupt appearance of novel biological forms by invoking "*Natura non facit saltum*" (Darwin, 1959; annotations by Costa in Darwin and Costa, 2009). Whether—or how often—novelties emerge and significantly influence the course of evolution (a proverbial leap of nature) immediately became a subject of debate among both Darwin's critics and supporters (Huxley 1860), and this debate has persisted through the Modern Synthesis era to the present (e.g., Simpson, 1944; Berry, 1985; Orr and Coyne, 1992; Wagner, 2014; Erwin, 2015; Jablonski, 2017). It remains unclear how impactful anatomical novelty (by any definition, see Moczek ,2008; Pigliucci, 2008; Peterson and Müller, 2013; Wagner, 2014) is on the evolutionary trajectory of a clade. This is particularly true of discrete structures that lack obvious homologous counterparts in predecessor taxa. While the loss, repetition, or extreme modification of anatomical features are recognized as potential mechanisms of functional and phylogenetic diversification (e.g., in vertebrates, the loss of limbs and repetition of the axial skeleton in snakes, Cohn and Tickle, 1999; Martill et al., 2015; or the modification of developing skin placodes in the evolution of feathers; Musser et al., 2015; Di-Poï and Milinkovitch, 2016), the paleontological and neontological records of evolution still contain neomorphic anatomical elements that are not well understood in terms of both their origin and evolution (e.g., in vertebrates, Hall, 2015).

Recent fossil discoveries have raised interest in one specific type of novel skeletal structure: the "styliform" elements of amniotes that use membranes to glide or fly (Fig. 1). This group of skeletal elements comprises the calcar of bats (Schutt and Simmons 1998), the styliform cartilages of gliding rodents and one marsupial (Coster et al., 2015; Kawashima et al., 2017; Johnson-Murray, 1987; Jackson, 2012), the pteroid of pterosaurs (Bennett, 2007), and was

recently expanded to include the styliform element of *Yi qi*, a maniraptoran theropod dinosaur (Xu et al., 2015) and the calcar of *Maiopatagium furculiferum*, a haramiyid mammaliaform (Meng et al., 2017). Since these skeletal rods are now known from disparate amniote lineages, they seem less like evolutionary oddities than consequential skeletal novelties characteristic of the skin membranes of volant body plans. The literature on most of these appendicular ossicles associated with skin membranes (Vickaryous and Olson, 2007) is limited to osteological descriptions (e.g., citations above), so much is still unknown about their function, origin, and diversification. The pterosaur pteroid has been the focus of several studies (summarized in Witton, 2013), but although the Pterosauria comprises a taxonomically diverse clade in which to explore pteroid variation, the lack of extant successors in the lineage restricts detailed anatomical and functional studies. In contrast, another of these neomorphic styliform elements—the bat calcar—is widespread across extant bats, making it an ideal model system for gaining a better understanding of the evolution of membrane-bound skeletal rods, and more generally, the evolution of neomorphic skeletal elements.

Bats (Chiroptera) are systematically, morphologically, and ecologically diverse (Simmons, 2005; Fenton and Simmons, 2015; Kunz and Fenton, 2005). The calcar articulates with the calcaneus in the bat ankle and extends into the membrane that spans between the two hindlimbs (Vaughan, 1970; Fig. 1). It abruptly appears in the early bat fossil record (*Onychonycteris finneyi*, Onychonycteridae, Green River Formation, WY, USA; ~52.5 Ma; Simmons et al. 2008) and, based on its ubiquity among extant bats, seems to have become fixed within the bat wing structure. In the terminology of evolutionary novelty, the calcar might be considered both a “novel character identity” or “Type I novelty” under the typology of Wagner (2014) and a “discrete new element added to an existing body plan” or “Type II novelty” under

the typology of Müller (2010). In addition, it meets Hall's (2015) definition of neomorphs, which "*seem to appear out of nowhere, de novo,* but are present in most if not all individuals of a species." The calcar is typically described as a bony or cartilaginous element, although histological studies to date have confirmed only the presence of cartilaginous tissue with varying levels of mineralization (Schutt and Simmons, 1998; Adams and Thibault, 1999; Czech et al., 2008; Stanchak and Santana 2018). Because bats are morphologically diverse and cartilage can be a precursor of bone, it has been hypothesized that the calcars of some bat species might be composed of bony tissue (Adams and Thibault, 1999).

The specific functions of the calcar are unknown, but it is generally described as providing support for the hindlimb membrane (Vaughan, 1970). However, bat hindlimbs have functions other than flight (e.g., roosting, and in some bats, prey capture, Novick and Dale 1971), so calcars may also take on different functions in species that vary ecologically. Functionally-diverse calcars should exhibit anatomical divergence based on differing functional requirements. For instance, in *Myotis*, long calcars were found to be associated with a trawling foraging strategy (Fenton and Bogdanowicz ,2002), and muscles associated with the calcar were found to vary anatomically in three species with different flight and foraging strategies (Stanchak and Santana, 2018).

In all animal clades with styliform elements, including bats, the evolution of membrane-bound limbs and a new locomotor mode (flight or gliding) allowed entry into new ecological space: the aerosphere. The bat fossil record demonstrates early taxonomic diversification coupled with a rapid expansion of their geographic distribution (Smith et al., 2012). Based on its presence in some of the earliest bat fossils (Simmons et al., 2008; Simmons and Geisler, 1998), the calcar may be part of the suite of adaptations that allowed bats to functionally and ecologically radiate

into varied niches after their initial invasion of the aerosphere. If so, we predict that (1) bat calcars will be morphologically diverse in trait parameters that theoretically affect function, and (2) calcar morphological diversification will reflect the rapid early diversification of Chiroptera, as suggested by the fossil record.

In this paper, we assess and describe the anatomical diversification of the calcar across the radiation of bats to test the predictions outlined above. We integrate a variety of methods to analyze calcar anatomy across a broad sample of bat species spanning diverse ecologies. First, we examine variation in the length of the calcar across Chiroptera and test different models of calcar evolution to reveal the macroevolutionary patterns and potential underlying processes that characterize calcar diversification. Then, we more closely investigate the anatomical diversity of the calcar with micro-Computed Tomography (μCT) scans to assess its status as a novel skeletal addition rather than another type of skeletal modification (e.g., a repeated tarsal element), and we integrate data from both μCT scans and histological sections to test the hypothesis that the calcar has histologically diversified. Finally, we combine gross dissections and diffusible iodine-based contrast-enhanced μCT (diceCT; Gignac et al., 2016) for the visualization of soft tissue to evaluate whether the calcars of all bats are homologous. These detailed anatomical studies inform the interpretations of the macroevolutionary modeling, allowing us to rigorously assess the scope and scale of bat calcar evolution.

MATERIAL AND METHODS

Calcar Length Measurements and Macroevolutionary Analyses

The length of a rod or shaft is one parameter that determines its ability to resist bending under an applied load (Hibbeler, 2007). Bat calcars generally take a rod-shaped form, so

comparisons of calcar length are informative about the potential functional importance of the calcar across bats. A single observer (KES) made caliper measurements of calcar, tibia, and forearm (i.e., radius) lengths of one-to-nine fluid-preserved specimens representing 226 species and all recognized families within Chiroptera. In total, the sample included 1,396 specimens with an average of six specimens per species. A list of museum specimens is provided as a spreadsheet in the Supporting Files. By measuring intact, fluid-preserved specimens, we ensured that any thin, cartilaginous portions of the calcar were present and measured. We rounded caliper measurements to the nearest 1mm to reflect imprecision in measuring skeletal features from external examination of intact specimens. Because we based all measurements on external examination of specimens, it is possible that a very small, not externally evident calcar resulted in assigning a value of 0 mm to the calcar length for some individuals (e.g., see Results regarding *Rhinopoma hardwickii*). We did not include fossil bat species in our sample because few postcrania are present in the bat fossil record and the calcars of some extant species are unmineralized, so we would not be able to confirm the absence of a calcar for any bat fossil species.

For each specimen, we calculated the ratio of the calcar length divided by either the tibia or the forearm length and then averaged these ratios across all specimens for a particular species to derive a unitless measure of hindlimb skeletal proportions to compare across species. We visualized the calcar-to-tibia length ratio character states on a pruned version of a relatively recent chiropteran phylogeny (Shi and Rabosky, 2015) using the "fastAnc" method of the "contMap" function (Felsenstein, 1985; Revell, 2013) from the *phytools* v.0.6 package (Revell, 2012) in R v.3.4.3 (R Core Team 2017; all analyses were performed in the same version of R). We also calculated the residuals of phylogenetic generalized least squares (pgls) regressions of

mean calcar length on mean tibia or mean forearm length assuming a Brownian motion correlation structure using the "phyl.resid" function (Revell, 2009; Revell, 2010) from the *phytools* v.0.6 R package (Revell, 2012). While the calcar-to-tibia length ratio is more intuitively relevant to calcar biomechanics and function–even beyond its use for size normalization–we used both the tibia and forearm ratios and pgls residuals in subsequent evolutionary analyses so that we could better interpret the effect of variable transformations on our model fits. In addition, we repeated all of the following analyses for datasets excluding the species for which we recorded a calcar length of 0 mm because a calcar was not externally visible on the specimens. We also repeated all of the following analyses using datasets from which we excluded the Old World fruit bats (Pteropodidae) due to their differing calcar anatomy. Pteropodid calcars are described as inserting on the tendon of the gastrocnemius muscle rather than articulating with the calcaneus and are consequently hypothesized to not be homologous to the calcars of other bats (Schutt and Simmons, 1998; Kobayashi, 2017). All data used in analyses are provided as a spreadsheet in the Supporting Files.

To gain insight on the evolutionary processes that may have led to extant calcar diversity, we fit three models of evolution (Brownian motion, early burst, and single-peak Ornstein-Uhlenbeck) to the calcar length ratios and pgls residuals using the "fitContinuous" function in the *geiger* v.2.0.6 R package (Harmon et al., 2007; Pennell et al., 2014). Brownian motion (BM) models a "random-walk" process in which the variance of a trait increases linearly through time (as defined in evolutionary modeling by the evolutionary rate parameter σ^2). It is often used to test the hypothesis of trait evolution under a drift or other random process (Felsenstein, 1973). The early burst (EB) model is used to test a niche-filling hypothesis consistent with an adaptive radiation; the rate at which a trait diversifies decreases with declining ecological opportunity

after an initial, rapid "early burst" of diversification (Blomberg et al., 2003; Harmon et al., 2010). The EB model is parameterized by the initial evolutionary rate (σ^2) and a parameter for the exponential change in evolutionary rates through time (a), such that when a = 0 the EB model reduces to the BM model and when a < 0 evolutionary rates decrease as time progresses (Harmon et al., 2007; Harmon et al., 2010). An Ornstein-Uhlenbeck (OU) process is used to model an evolutionary process in which some restoring force (e.g., selection; parameterized by α) restrains a trait value (θ) through time (Hansen, 1997; Butler and King, 2004). As implemented here, the model assumes a single optimal trait value that is equal to the root ancestral state of the trait (Harmon et al., 2007; parameterized by z_0 in all models). We compared these three models using small sample size-corrected Akaike weights (w_{AICc}). If the calcar underwent an early morphological diversification as the first bats phylogenetically diversified, we expected to find the highest support for the EB model.

To visualize and quantify the tempo of calcar length evolution, we performed a disparity-through-time analysis using the "dtt" function (Harmon et al., 2003; Slater et al., 2010) from the *geiger* v.2.0.6 R package (Harmon et al., 2007; Pennell et al., 2014) to calculate the mean morphological disparity of each subtree in the pruned phylogeny using the average squared Euclidean distance among all pairs of points. We plotted this curve against a null distribution created by using the same procedure on a set of 1,000 simulations across the pruned phylogeny assuming a BM model of evolution of the relative calcar lengths. We used the morphological disparity index (MDI) to quantitatively compare subclade disparity in relative calcar length with the disparity expected under a BM model (Harmon et al., 2003; Slater et al., 2010). We determined the significance of the MDI by the frequency at which a calculated MDI between the data set and each simulation trial was greater than zero. A negative MDI value indicates that

disparity is partitioned more strongly among early divergence events, with more recent subclades each representing only a small portion of the total morphological diversity of the clade than expected under a constant-rate, random walk process (e.g., BM; Harmon et al., 2003; Slater et al., 2010). Positive MDI values may be indicative of selective constraint or increasing evolutionary rates, where each recent subclade is more likely to represent a greater proportion of trait space (López-Fernández et al., 2013). A negative MDI supports a hypothesis of early, rapid morphological diversification prior to a period of relative stasis until the present day (Slater et al., 2010). To more rigorously assess the prediction of early disparification, we also calculated the MDI between the dtt curve and a curve distribution simulated under an EB model of evolution (Slater and Pennell, 2014). We would expect these MDI values to be higher than those calculated against the BM simulations, as we expect calcar length evolution to more closely emulate an EB pattern of disparification than a BM pattern. Text of all R code is provided in the Supporting Information.

CT Scanning

To examine calcar anatomy in the context of other ankle and foot bones across bat species, we dissected and μCT scanned one foot of each of 19 fluid-preserved bat specimens representing 13 families within Chiroptera. We also μCT scanned three whole (non-dissected) fluid-preserved specimens representing three additional bat families (listed in Supporting Information) for a total sample of 22 species representing 16 families. These specimens were sourced from museum collections, research collections in the Santana Lab and the Herring Lab at the University of Washington, and the Lubee Bat Conservancy. We segmented (digitally-dissected) the tarsals, the calcar, and other accessory ossicles in each μCT scan using Mimics

v.19 (Materialise). The resulting 3D renderings allowed us to compare tarsal osteology across our samples in unprecedented detail.

Previous studies of pteropodid calcar anatomy describe a calcar that inserts on the tendon of the gastrocnemius muscle. This tendon then inserts on the calcaneal tuberosity. In contrast, calcars of the other bat families articulate directly with the calcaneus; thus, it has been hypothesized that the pteropodid calcars are not homologous to the calcars of other bats (Schutt and Simmons, 1998). In previous phylogenetic hypotheses, Pteropodidae was considered the sister clade to all of the other bat families, which were collectively referred to as the "microchiroptera." However, after the phylogeny of Chiroptera was revised using molecular data, non-pteropodid bats were rendered paraphyletic (Teeling et al., 2005). As a consequence, the hypothesis of a lack of homology between the pteropodid calcar and that of the "microbats" became a less-parsimonious explanation than that of a homologous calcar across Chiroptera. To better assess the soft tissue morphology of the calcars in the Pteropodidae, we used diffusible-iodine contrast-enhanced μCT scanning (diceCT, Gignac et al., 2016) and conventional μCT scanning to image the feet of the three pteropodid species in our sample. For diceCT scanning, we placed each fluid-preserved specimen in a solution of Lugol's iodine (3% total solute) for two to three days prior to CT scanning. The iodine solution increases the x-ray opacity of soft tissue—particularly muscle—in the sample, allowing for the visualization of this tissue in the μCT scan. Then, we dissected each of the pteropodid feet to further assess the connection between the calcar spur and the calcaneus. A list of scanned specimens and μCT scanner settings is provided in the Supporting Information at the end of this chapter.

Histology

We used both the μCT scans and histological sections of the dissected specimens to compare calcar tissue composition across 18 bat species (listed in Supporting Information). Calcified calcar samples were first decalcified in 14% EDTA aqueous solution neutralized with ammonium hydroxide. Because we had difficultly completely decalcifying some samples in EDTA, we transferred them to 5% aqueous formic acid for further decalcification. We then dehydrated, cleared, and embedded all samples in paraffin wax. We sectioned each paraffin block at 5-8 μm with a Leica RM2145 microtome, mounted the sections to slides, then cleared, rehydrated, and stained the sections using either modified Mayer's hematoxylin and Mallory's triple connective tissue stain (Humason, 1962) or Weigert's iron hematoxylin and fast green/safranin O. For all samples, we determined calcar tissue composition by cell and substrate morphology, not by stain color. We imaged the sections with a Nikon Eclipse E600FN compound microscope and an AmScope MU300 camera.

RESULTS

The calcar exhibits extensive anatomical diversity across Chiroptera. Calcars range from not externally visible (a length of zero) to considerably longer than the tibia (Fig. 2). We found strong support ($w_{AICc} > 0.99$) for the EB model of morphological evolution for calcar length relative to tibia length in all model comparisons that included pteropodid bats in the sample (Table 1). All OU models collapsed to BM models, so only model results for BM and EB models are shown. Support for the EB model decreased for the sample that did not include Pteropodidae, but our diceCT and dissection-based anatomical observations suggest that the calcars of pteropodid bats vary morphologically, and some variants resemble the morphologies of the non-

pteropodid bats (see detailed anatomical descriptions below). Thus inclusion of the Pteropodidae in these phylogenetic analyses is justified. Disparity-through-time analyses supported early diversification of calcar length in all cases, as evidenced by significantly low MDI values when compared to a null BM distribution (Fig. 3, Table 2). MDI values consistently increased when the calcar length disparity-through-time curve was compared to a distribution generated under an EB model of evolution.

Detailed investigation of calcar anatomy with μCT scans revealed that bat ankles exhibit numerous tarsal modifications and collectively contain multiple accessory ossicles (Fig. 4; descriptions in Supporting Information). However, none of these osteological modifications refute the status of the calcar as a neomorphic skeletal structure or morphological novelty. In no bat species is the calcar contiguous with another tarsal, nor is the calcar an obviously repeated skeletal element. The calcar of any one bat species is only anatomically similar in both structure and location to calcars of other bats and not to another tarsal element.

Histological sections complemented the μCT scans in revealing tissue-level diversity in bat calcars. While calcars are predominantly composed of uncalcified or calcified cartilage, some calcars contain ossified tissue (Fig. 5; Supporting Information). The calcar of *Noctilio leporinus* (Noctilionidae; FHA 1651) is composed of thick cortical bone in the section proximal to the ankle, and both μCT scans and histological sections demonstrated the formation of trabeculae (Fig. 5a, b, c). The type of connective tissue also varies within a single calcar, along a continuum of cartilage, calcified cartilage, and bone. The calcar of *Molossus molossus* (Molossidae; FHA 1857) is bony proximately and cartilaginous distally; as the bone grades into cartilage, only the interior of the calcar shaft is bony, and this bony tissue is surrounded by a thick layer of tissue that appears more cartilage-like (Fig. 5d, e). This partially bony calcar contrasts with the typical

cartilaginous calcar of other species, as exemplified by the primarily calcified cartilage calcar of *Eptesicus fuscus* (Vespertilionidae; Santana Lab KES 037; Fig. 5f). Both the *E. fuscus* and *M. molossus* calcars are surrounded by a thick, perichondrium-like envelope (Fig. 5e and 5f, respectively). *Pteronotus quadridens* (Mormoopidae; FHA 780) and *Macrotus waterhousii* (Phyllostomidae; FHA 135) also have bony proximal ends of their calcars, but the degree to which this ossification extends distally varies between the two species (Appendix S1). The short calcar of *Desmodus rotundus* (Phyllostomidae; Santana Lab 022714-06) also exhibits bony tissue (Fig. 5g).

Histological sections also confirmed the presence of a synovial joint between the calcar and the calcaneus in several bat species (Fig. 5e, f, g; Supporting Information) and the presence of a relatively small, uncalcified, cartilaginous calcar in one species in which the calcar was thought to be absent (*Rhinopoma hardwickii*, Rhinopomatidae; FMNH 123185; Fig. 5h). Our anatomical analyses also highlighted known shape differences across bat calcars; although most calcars take the form of a rod with an approximately elliptical cross-section, some exhibit notably divergent shapes. For example, a cartilaginous hook-like "keel" structure protrudes from the main shaft of the calcar in some species, including *Eptesicus fuscus*, *Myotis californicus* (Vespertilionidae; Santana Lab KES 026), and *Thyroptera tricolor* (Thyropteridae; MVZ 158246). The bony portion of the calcar of *Noctilio leporinus* exhibits an antero-posteriorly flattened cross-section with multiple cavities in the bony tissue (Fig. 5b). We describe, for the first time, that the calcar of *Mystacina tuberculata* (Mystacinidae; MVZ 173918) has two distinct calcified tines (Fig. 4e, f), a unique morphology among the calcars in our sample.

The diceCT scans and dissections of pteropodid feet revealed calcar anatomical diversity within the Pteropodidae. The diceCT scan of *Cynopterus brachyotis* (Pteropodidae; UWBM

82863) indicates that the calcar and the tendon of the gastrocnemius muscle make two separate, distinct insertions on the calcaneal tuberosity. We confirmed this observation through a dissection in which we were able to cleanly pass a pin between the insertions of the calcar and the tendon on the calcaneus (Fig. 5). However, dissections of the calcars of *Rousettus aegyptiacus* (Herring Lab 224) and *Pteropus* sp. (Herring Lab 76) indicated that the calcar tissue is contiguous with the tendon of the gastrocnemius muscle. DiceCT scans of these species were inconclusive, as iodine solution only slightly increases CT scan image contrast in cartilage. More detailed anatomical descriptions of each species examined with μCT scanning and histological sectioning are provided in Supporting Information.

DISCUSSION

The bat calcar is a skeletal novelty that has anatomically diversified widely throughout Chiroptera. This diversification appears to have occurred early in chiropteran history, as evidenced by support for an early burst model of calcar length evolution and the corresponding negative morphological disparity indices. This is consistent with evidence for early diversification of bats in the fossil record (Smith et al., 2012) and an overall declining rate of speciation in Chiroptera (Shi and Rabosky, 2015). Specimens referred to the Onychonycteridae, one of the earliest bat families, have been found on both the North American and Eurasian Eocene landmasses (Hand et al., 2015). By the end of the Eocene, bats are known from six continental land masses (Smith et al., 2012; Hand et al., 2015). Eocene bat postcrania are best preserved in the Green River Formation of WY, USA and the famous Messel Lagerstätten near Messel, Germany. *Onychonycteris finneyi*, which represents the earliest-known record of a calcar, also had intermediate postcranial characteristics, with limb proportions between those of

bats and non-volant mammals (Simmons et al., 2008). However, no calcars have been found in postcranial fossils of *Icaronycteris index*, another Green River bat like *O. finneyi*, but with limb proportions typical of some extant bats. Among the Messel bats, *Hassianycteris*, *Palaeochiropteryx*, and *Tachypteron* had calcars, but no calcars have been reported in specimens of *Archaeonycteris* (Simmons and Geisler, 1998; Storch et al., 2002). Additionally, no evidence of an articulation facet has been found on the calcanei of *Icaronycteris* and *Archaeonycteris* (Simmons and Geisler, 1998). Because calcars vary in amount of calcification, it is possible that uncalcified cartilage calcars were not preserved in these taxa; nonetheless, it is clear that Eocene bats exhibited diversity in either the presence of a calcar or in the amount of calcar calcification soon after the first bats evolved flight.

We found weaker support for the EB model when only non-pteropodid calcars were included in the analyses. However, our pteropodid diceCT scan and dissection results call into question the proposition that the pteropodid calcar is not homologous to the calcar of other bats. We have demonstrated that the calcar morphology of at least one pteropodid individual (*Cynopterus brachyotis*) differs from the calcar morphology of other pteropodids; its relation to the surrounding connective tissue makes it more similar to the "microbat" calcar condition. This intermediate anatomical condition in *C. brachyotis* suggests that it is more appropriate to consider the calcars of all bats in macroevolutionary analyses, rather than just those of the paraphyletic "microchiroptera."

Support for the EB model of morphological evolution is notoriously low in the macroevolution literature (Harmon et al., 2010). It has been proposed that this could be an artefact of either hypothesis testing at too low of a taxonomic level, such that the signal of the "early burst" of the higher-level clade has been lost, or a consequence of testing variables that

are not functionally-linked to the specific radiation, such as body mass and overall shape (Slater and Friscia, 2019). The evolution of wings in the early Chiroptera is a type of extensive morphological change that would be expected to precede a burst of diversification, as flight would allow access to an entirely new ecospace (other examples summarized in Erwin, 2015). The calcar abruptly appeared in the fossil record as part of this wing structure and is now found in the vast majority of bats. When we tested an early burst hypothesis of calcar evolution across all of Chiroptera, we found that the calcar—a distinct synapomorphy associated with an aerial ecological mode—retains the signal of an early diversification burst. The true key innovation, however, is likely the full wing apparatus, which not only includes the novel calcar but also the elongation of the forelimb bones and the evolution of novel and developmentally-retained wing membranes.

Across extant bats, the calcar exhibits interspecific diversity in anatomical parameters that are likely to affect function, both in terms of overall structure (e.g., length and shape) and material (histological) composition. Although others have noted differences in the amount of calcar calcification among species based on dissection observations and clearing and staining procedures (Schutt and Simmons, 1998; Koyabu and Son, 2014; Reyes-Amaya et al., 2017), this is the first study to histologically confirm the presence of ossified tissue in the bat calcar. Given that there is extensive variation in material properties between cartilage, calcified cartilage, and bone (Currey, 2002), interspecific variation in calcar tissue composition, length, and/or shape would result in interspecific differences in responses to applied loading (e.g., muscular contraction or resistance of a stretched membrane). Additionally, the presence of a synovial joint between the calcar and the calcaneus, in combination with the presence of skeletal muscles that insert on the calcar (Schutt and Simmons, 1999; Glass and Gannon, 1994; Stanchak and Santana,

2018), suggests a kinematic functional role for the calcar. Although there are reported observations of moving calcars (e.g., in *Noctilio leporinus* as they trawl bodies of water for fish prey; Vaughan, 1970; Altenbach, 1989), calcar motion has not yet been confirmed with a rigorous kinematic analysis in any bat species. Further detailed, quantitative analyses of calcar biomechanics, including material testing and behavioral experiments, are required to estimate the magnitude of the effect of anatomical variation on any potential calcar function.

The developmental origin of the calcar is still a mystery. Although the immediate ancestry of the chiropteran lineage is unknown (Halliday et al., 2017), no calcar-like structure is found in earlier eutherian mammals. However, the discovery of a calcar in a Mesozoic mammaliaform (Meng et al., 2017) raises the possibility of a deep homological explanation for the origin of the calcar (Shubin et al., 2009). One hypothesis for calcar development is that it initially develops within existing connective tissue in the hindlimb membrane via a process of metaplasia (Carter and Beaupré, 2007). The condition of the pteropodid calcar, as described here, may provide incremental support for this hypothesis. Connective tissue (cartilage, tendon, and even bone) is both plastic and labile (Hall, 2015). The calcar may have arisen in a mass of connective tissue in close proximity to the calcaneus, perhaps as that mass of tissue was placed under stress during the development of the hindlimb membrane. Consequently, differences among species in the association of the calcar with the calcaneus may be the result of relatively minor developmental alterations. Our finding of many sesamoids in bat feet, consistent with a recent assessment of bat sesamoids (Amador et al., 2018), suggests a propensity for metaplastic cartilage and bone development in bat feet, as tendon metaplasia is hypothesized to play a role in sesamoid development (Sarin et al., 2002; but see also Eyal et al., 2015, 2019). Developmental plasticity may also lead to intraspecific variation in calcar anatomy or even presence. This might

be a fruitful path of further study in light of our finding of a small, calcar-like structure in the foot of one specimen of *Rhinopoma hardwickii*.

The skeletal ossicles associated with skin membranes of mammals are under-explored in studies of morphological evolution (Vickaryous and Olson, 2007). The bat calcar is an anatomically diverse skeletal novelty found in a vast majority of species of a highly diverse clade of mammals. It evolved into a potentially functionally-important part of the bat wing, morphologically diversifying during the early radiation of bats, which lends support to the idea that evolutionary novelty can, in some cases, precede and prompt adaptive radiations. Additional, focused studies of the bat calcar—especially of its function and development—have a high potential to yield new knowledge of skeletal biology and a better understanding of the mechanisms through which the skeleton evolves into novel forms.

TABLES

Table 1. Results from evolutionary model comparisons. Calcar/Tibia and Calcar/Forearm indicate models considering ratios of calcar length to tibia and forearm length, respectively; Calcar~Tibia and Calcar~Forearm indicate models using residuals of phylogenetic regressions of the same variables. BM = Brownian motion model; EB = Early Burst model; a, σ^2, and z0 are the fit parameters of those models corresponding to the names used in the "fitContinuous" function (see Material and Methods); w_{AICc} = AIC_c weights. All OU models collapsed to BM models, so only BM and EB results are shown. Bold text emphasizes models with $w_{AICc} > 0.99$.

	Model	σ^2	z0	a	w_{AICc}	ΔAIC_c
Calcar/Tibia						
all data	BM	0.0011	0.7073	--	<0.001	23.579
	EB	**0.0056**	**0.6872**	**-0.0434**	**>0.999**	**0**
no zero lengths	BM	0.0010	0.7568	--	<0.001	16.167
	EB	**0.0041**	**0.7524**	**-0.0374**	**>0.999**	**0**
no zero lengths or Pteropodidae	BM	0.0010	0.8348	--	0.0477	5.952
	EB	0.0034	0.8313	-0.0299	0.9353	0
Calcar/Forearm						
all data	BM	0.0002	0.2854	--	<0.001	22.207
	EB	**0.0008**	**0.2787**	**-0.0416**	**>0.999**	**0**
no zero lengths	BM	0.0001	0.3055	--	0.0009	13.962
	EB	**0.0005**	**0.3053**	**-0.0345**	**0.9987**	**0**
no zero lengths or Pteropodidae	BM	0.0002	0.3373	--	0.1415	3.485
	EB	0.0004	0.3374	-0.0252	0.8081	0
Calcar ~ Tibia						
all data	BM	0.4344	0.0	--	<0.001	20.036
	EB	**2.1063**	**-0.3221**	**-0.0412**	**>0.999**	**0**
no zero lengths	BM	0.3899	0.0	--	0.0007	14.395
	EB	**1.6065**	**-0.0694**	**-0.0365**	**0.9990**	**0**
no zero lengths or Pteropodidae	BM	0.3491	0.0	--	0.1577	3.212
	EB	0.8923	-0.0675	-0.0234	0.7861	0

…continued on next page

Calcar ~ Forearm						
all data	BM	0.4489	0.0	--	<0.001	16.869
	EB	**1.9658**	**-0.2503**	**-0.0383**	**>0.999**	**0**
no zero lengths	BM	0.4092	0.0	--	0.0038	11.149
	EB	**1.4769**	**-0.0112**	**-0.0328**	**0.9949**	**0**
no zero lengths or Pteropodidae	BM	0.3763	0.0	--	0.3999	0.270
	EB	0.7381	0.0004	-0.0165	0.4577	0

Table 2. Results from disparity-through-time analyses. MDI = morphological disparity index; BM = Brownian motion model; EB = Early Burst model.

	MDI (BM)	MDI (EB)
Calcar/Tibia		
all data	-0.284 ($p < 0.001$)	-0.105 ($p = 0.034$)
no zero lengths	-0.275 ($p < 0.001$)	-0.119 ($p = 0.036$)
no zero lengths or Pteropodidae	-0.236 ($p = 0.002$)	-0.112 ($p = 0.063$)
Calcar/Forearm		
all data	-0.287 ($p < 0.001$)	-0.113 ($p = 0.023$)
no zero lengths	-0.278 ($p < 0.001$)	-0.125 ($p = 0.013$)
no zero lengths or Pteropodidae	-0.223 ($p = 0.001$)	-0.113 ($p = 0.065$)
Calcar ~ Tibia		
all data	-0.223 ($p < 0.001$)	-0.056 ($p = 0.182$)
no zero lengths	-0.221 ($p = 0.001$)	-0.066 ($p = 0.161$)
no zero lengths or Pteropodidae	-0.195 ($p = 0.003$)	-0.0898 ($p = 0.108$)
Calcar ~ Forearm		
all data	-0.222 ($p = 0.001$)	-0.055 ($p = 0.195$)
no zero lengths	-0.207 ($p = 0.004$)	-0.075 ($p = 0.128$)
no zero lengths or Pteropodidae	-0.17 ($p = 0.027$)	-0.093 ($p = 0.129$)

FIGURES

Figure 1. (on next page) Neomorphic skeletal rods have evolved multiple times in vertebrates with gliding or flying membranes. These structures are indicated in pink in the schematic drawing. Drawings based on Xu et al. 2015, Meng et al. 2017, Bennett 2007, Witton 2013, Coster et al. 2015, Kawashima et al. 2017, Johnson-Murray 1987, Jackson 2012.

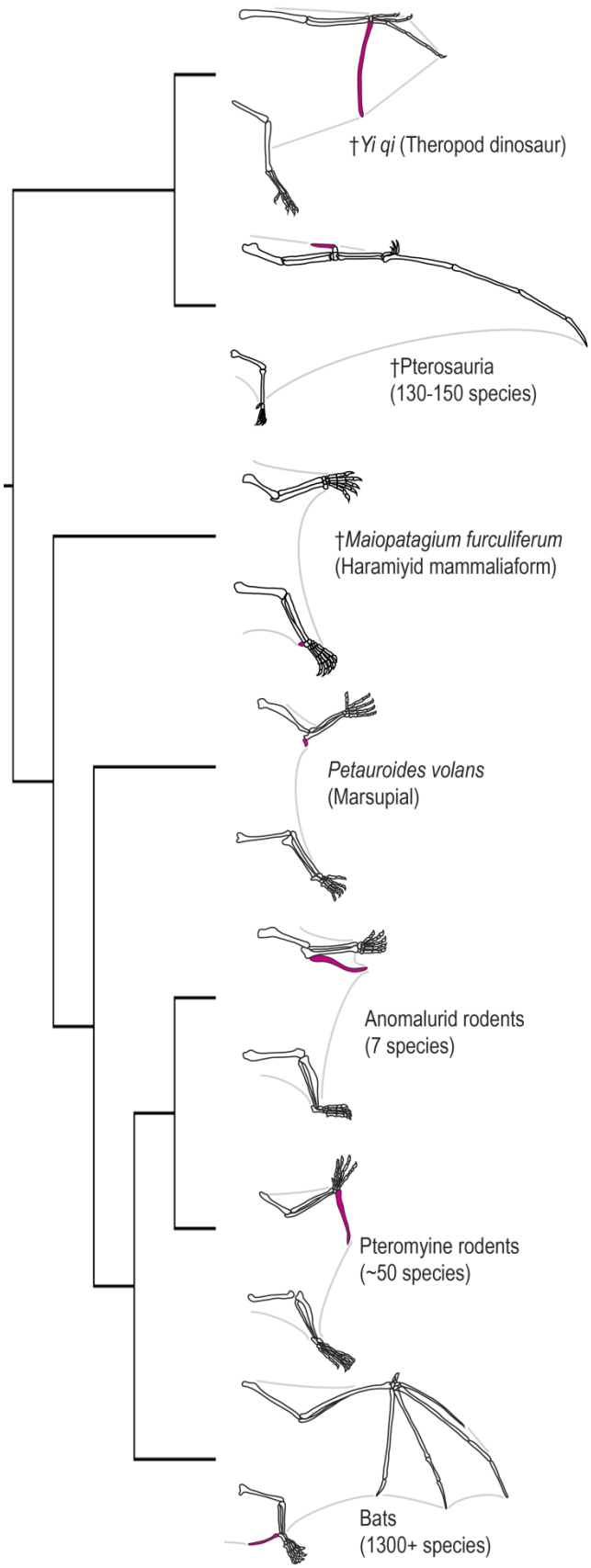
†*Yi qi* (Theropod dinosaur)
†Pterosauria
(130-150 species)
†*Maiopatagium furculiferum*
(Haramiyid mammaliaform)
Petauroides volans
(Marsupial)
Anomalurid rodents
(7 species)
Pteromyine rodents
(~50 species)
Bats
(1300+ species)

Figure 2. Relative calcar length varies extensively and diversified early in bat evolutionary history. Ratio of calcar length-to-tibia length is plotted on a phylogeny of Chiroptera (Shi and Rabosky 2015). Gray lines around the phylogenetic tree designate bat families; species-rich families are labeled. Schematic drawing on the color scale illustrate representative hindlimb morphologies for different calcar lengths.

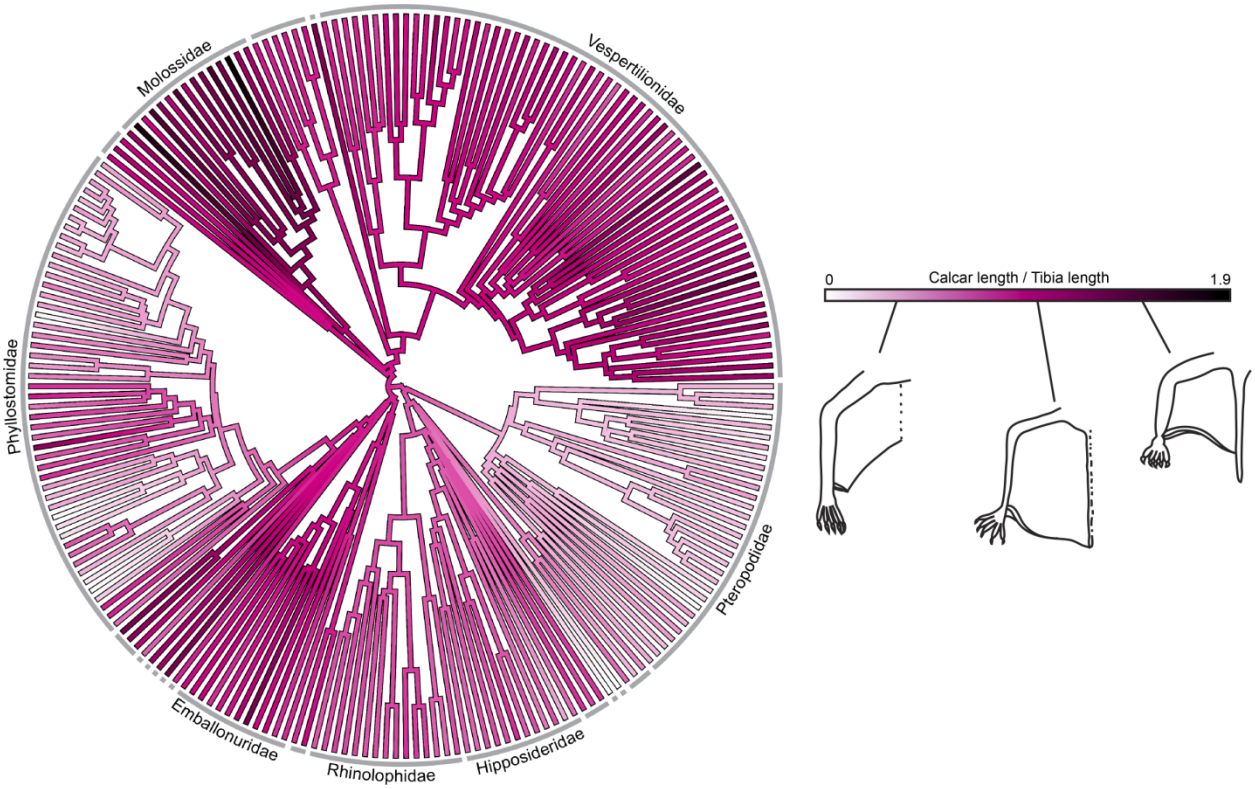

Figure 3. A disparity-through-time analysis supports an early burst of calcar length evolution. The black line indicates the mean subclade disparity through time for the measured calcar-to-tibia length ratios, the dotted line is the mean subclade disparity through time for 1,000 Brownian motion simulations, and the gray band indicates a 95% confidence range for the simulations.

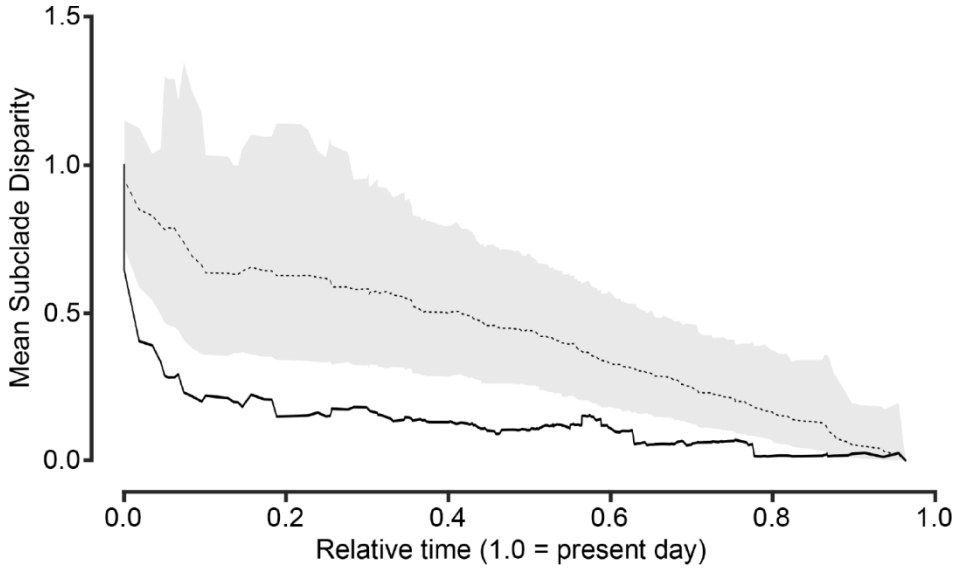

Figure 4. Bat ankle morphologies as demonstrated by rendered µCT scans. (a) Ankle of *Balantiopteryx plicata* (Santana Lab 0229-06), demonstrating calcar-calcaneus articulation (in pink-yellow), the other typical mammalian tarsals (in addition to the calcaneus; in shades of gray), and an additional sesamoid (in green). Inset demonstrates the ankle position relative to the full leg. Other bat feet µCT scans pictured are (b) *Noctilio leporinus* (FHA 1651), (c) *Desmodus rotundus* (Santana Lab 022714-06), (d) *Rhinolophus affinis* (AMNH 234034; calcar not visible due to lack of calcification), (e and f) *Mystacina tuberculata* (MVZ 173918). All are pictured in plantar view except (f), which is medial to show calcified tines on calcar.

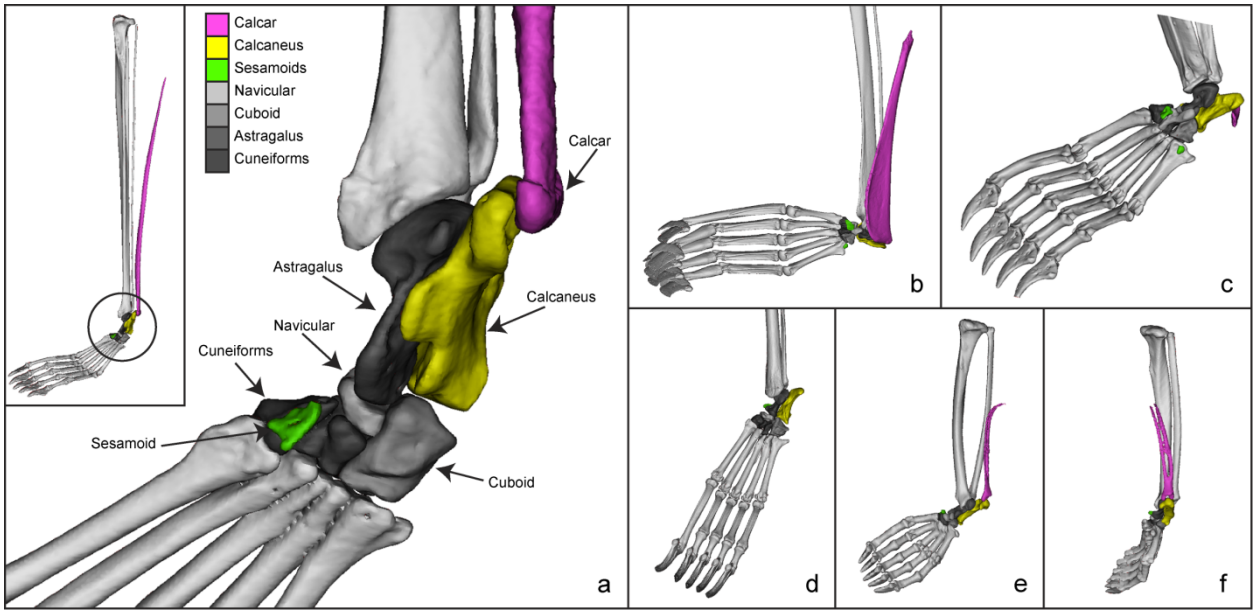

Figure 5. (on next page) Histological diversity in the bat calcar. (a) Slice of μCT scan through the longitudinal axis of the calcar of *Noctilio leporinus* (FHA 1651). (b) Axial μCT scan slice through the hindlimb of *N. leporinus*, demonstrating cross-sectional shapes of the calcar and leg bones. (c) Mallory-stained histological section through the ankle of *N. leporinus*, demonstrating bony calcar tissue and a ligamentous connection between the calcar and calcaneus. (d) Slice of μCT scan and (e) fast green/safranin O-stained histological section through the longitudinal axis of the calcar of *Molossus molossus* (FHA 1857), demonstrating bony tissue in the calcar near the synovial joint with the calcaneus, which then transitions distally to calcified cartilage. (f) Fast green/safranin O-stained histological section of *Eptesicus fuscus*, showing a fully-cartilaginous calcar and a synovial joint between the calcaneus and the calcar. (g) Mallory-stained histological section of *Desmodus rotundus* (Santana Lab 022714-06), demonstrating bony nodule of calcar near the synovial articulation with the calcaneus. (h) Mallory-stained histological section demonstrating calcar presence in *Rhinopoma hardwickii* (FMNH 123185). Ca = calcar, Cs = calcaneus, Fi = fibula, Ti = tibia. In all sections the scale bar indicates 100μm, except for (a) and (b) where it is 500μm.

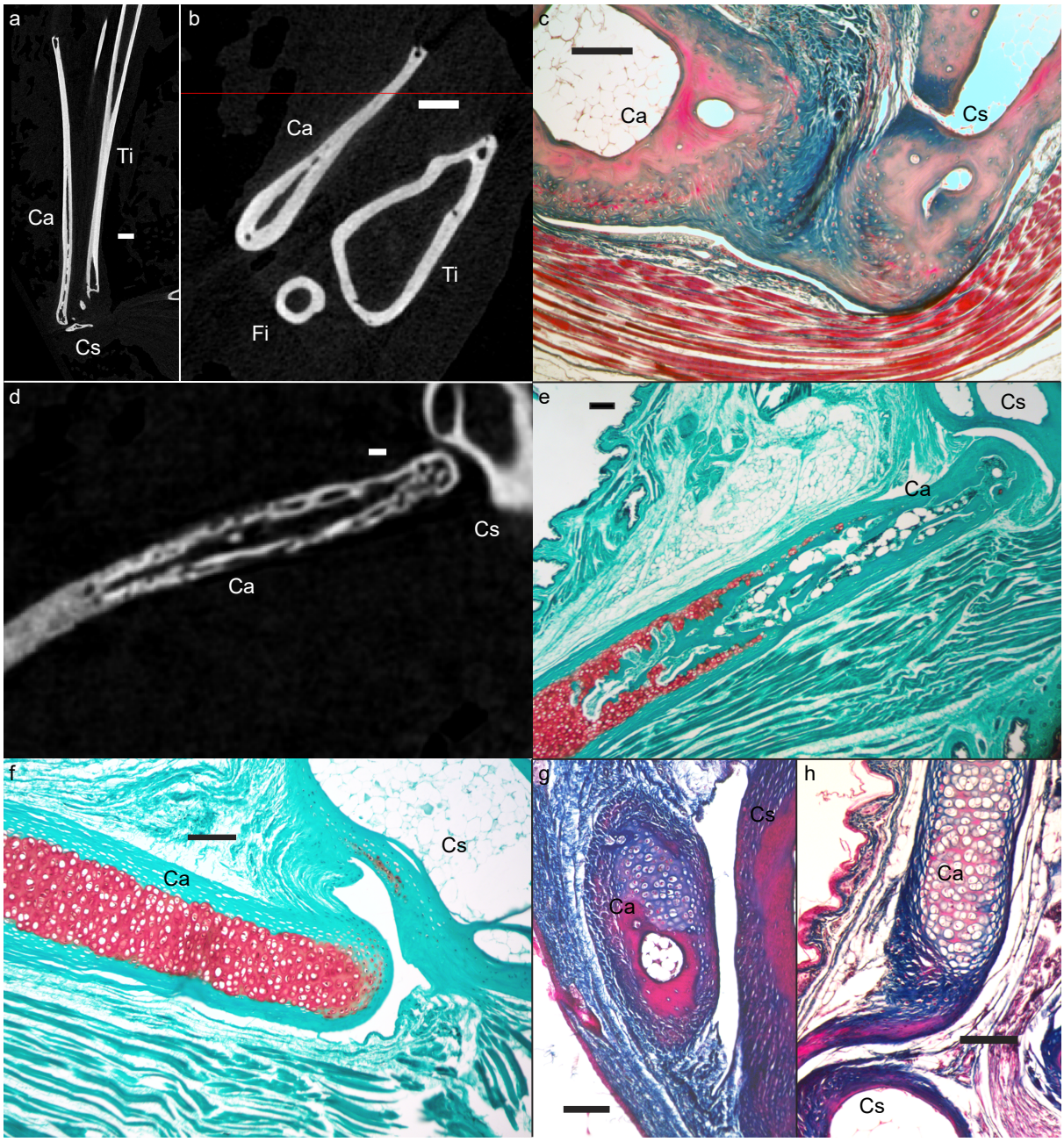
a
Ti
Ca
Cs
b
Ca
Ti
Fi
c
Ca
Cs
d
Cs
Ca
e
Cs
Ca
f
Ca
Cs
g
Cs
Ca
h
Ca
Cs

Figure 6. Photographs of dissection of the *Cynopterus brachyotis* (UWBM 82863) ankle, demonstrating separation between the calcar and the tendon of the gastrocnemius muscle. (a) – (c) are dissection photos of an iodine-stained specimen. (b) pin demonstrates the separation between the calcar and the tendon. (c) shows the insertion of the calcar on the calcaneal tuberosity after the tendon has been dissected out. (d) is a slice of the diceCT scan demonstrating the separation between the calcar and the tendon and their two distinct insertions on the calcaneus. Ca = calcar, Cs = calcaneus, tm = tendon of the gastrocnemius muscle.

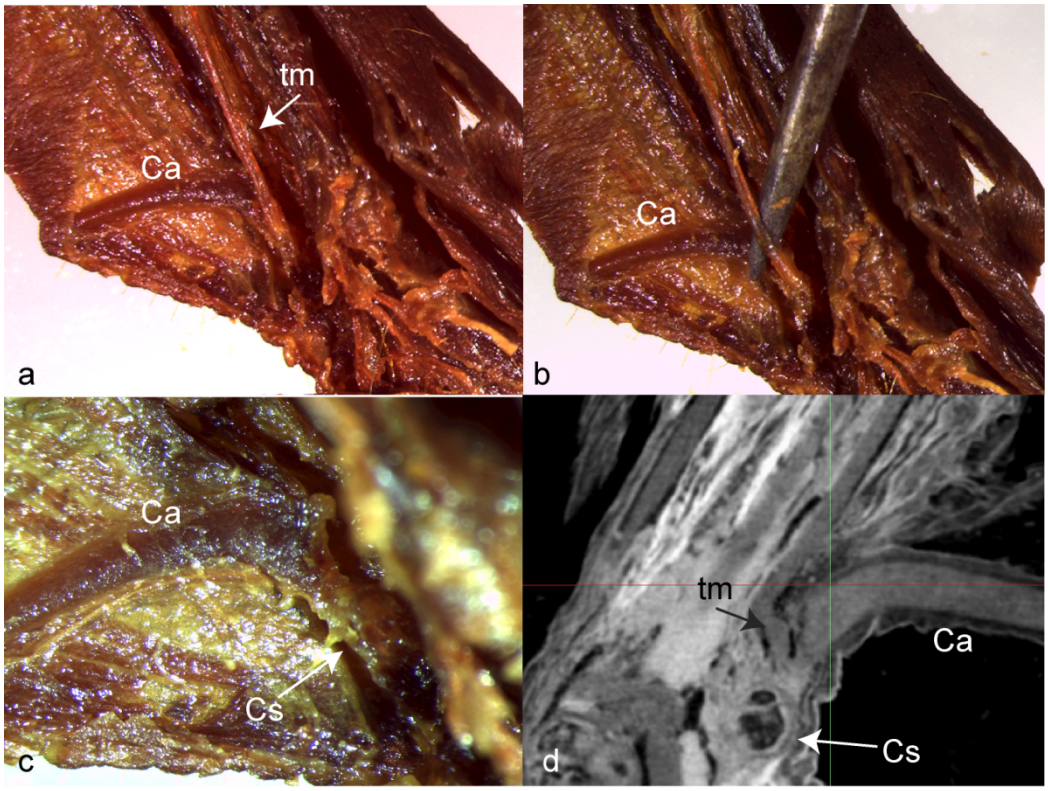

REFERENCES

Adams, R.A., and K. M. Thibault. 1999. Growth, development, and histology of the calcar in the little brown bat, Myotis lucifugus (Vespertilionidae). Acta chiropterol. 1:215-221.

Altenbach, J.S. 1989. Prey capture by the fishing bats Noctilio leporinus and Myotis vivesi. J. Mammal. 70:421-424.

Amador, L.I., Giannini, N.P., Simmons, N.B., and V. Abdala. 2018. Morphology and evolution of sesamoid elements in bats (Mammalia: Chiroptera). Am. Mus. Nov. 3905:1-40.

Bennett, S.C. 2007. Articulation and function of the pteroid bone of pterosaurs. J. Vertebr. Paleontol. 27:881-891.

Berry, R. J. 1985. Natura non facit saltum. Biol. J. Linn. Soc. 26:301-305.

Blomberg, S.P., Garland Jr., T., and A.R. Ives. 2003. Testing for phylogenetic signal in comparative data: Behavioral traits are more labile. Evolution 57:717-745.

Butler M.A., and A.A. King. 2004. Phylogenetic comparative analysis: a modeling approach for adaptive evolution. Am. Nat. 164:683-695.

Carter, D.R., and G.S. Beaupré. 2007. *Skeletal function and form: mechanobiology of skeletal development, aging, and regeneration*. Cambridge Univ. Press.

Cohn , M.J., and C. Tickle. 1999. Developmental basis of limblessness and axial patterning in snakes. Nature 399:474-479.

Coster, P., Beard, K.C., Salem, M.J., Chaimanee, Y., and J.J. Jaeger. 2015. New fossils from the Paleogene of central Libya illuminate the evolutionary history of endemic African anomaluroid rodents. Front. Earth Sci. 3:56.

Currey, J.D. 2002. *Bones: structure and mechanics*. Princeton Univ. Press.

Czech, N.U., Klauer, G., Dehnhardt, G., and B.M. Siemers. 2008. Fringe for foraging? Histology of the bristle-like hairs on the tail membrane of the gleaning bat, Myotis nattereri. Acta chiropterol. 10:303-311.

Darwin, C. 1859. *On the Origin of Species by Means of Natural Selection*. J. Murray, London.

Darwin, C., and J.T. Costa. 2009. *The annotated Origin: a facsimile of the first edition of On the origin of species*. Harvard Univ. Press.

Di- Poï, N., and M.C. Milinkovitch. 2016. The anatomical placode in reptile scale morphogenesis indicates shared ancestry among skin appendages in amniotes. Science advances 2:e1600708.

Erwin, D.H. 2015. Novelty and innovation in the history of life. Curr. Biol. 25:930-940.

Eyal, S., Blitz, E., Shwartz, Y., Akiyama, H., Schweitzer, R., and E. Zelzer. 2015. On the development of the patella. Development 142:1831-1839.

Eyal, S., Rubin, S., Krief, S., Levin, L., and E. Zelzer. 2019. Common cellular origin and diverging developmental programs for different sesamoid bones. Development 146:dev167452. .

Felsenstein, J. 1973. Maximum likelihood estimation of evolutionary trees from continuous characters. Am. J. Hum. Genet. 25:471-492.

Felsenstein, J. 1985. Phylogenies and the comparative method. Am. Nat. 125:1-15.

Fenton, M.B., and W. Bogdanowicz. 2002. Relationships between external morphology and foraging behavior: bats in the genus Myotis. Can. J. Zool. 80:1004-1013.

Fenton, M.B., and N.B. Simmons. 2015. *Bats: A World of Science and Mystery*. Univ. of Chicago Press.

Gignac, P.M., Kley, N.J., Clarke, J.A., Colbert, M.W., Morhardt, A.C., Cerio, D., Cost, I.N., Cox, P.G., Daza, J.D., Early, C.M., and M.S. Echols. 2006. Diffusible iodine-based contrast-enhanced computed tomography (diceCT): an emerging tool for rapid, high-resolution, 3-D imaging of metazoan soft tissues. J. Anat. 228:889-909.

Glass, P.J., and W.L. Gannon. 1994. Description of M. uropataginalis (a new muscle), with additional comments from a microscopy study of the uropatagium of the fringed myotis (Myotis thysanodes). Can. J. Zool. 72:1752-1754.

Hall, B.K. 2015. *Bones and Cartilage*. Academic Press.

Halliday, T.J.D., Upchurch, P., and A. Goswami. 2017. Resolving the relationships of Paleocene placental mammals. Biol. Rev. 92:521-550.

Hand, S.J., Sigé, B., Archer, M., Gunnell, G.F., and N.B. Simmons. 2015. A new early Eocene (Ypresian) bat from Pourcy, Paris Basin, France, with comments on patterns of diversity in the earliest chiropterans. J. Mamm. Evol. 22:343-354.

Hansen, T.F. 1997. Stabilizing selection and the comparative analysis of adaptation. Evolution 51:1341-1351.

Harmon, L.J., Schulte, J.A., Losos, J.B., and A. Larson. 2003. Tempo and mode of evolutionary radiation in igunaian lizards. Science 301:961-964.

Harmon, L.J., Weir, J.T., Brock, C.D., Glor, R.E., and W. Challenger. 2007. GEIGER: investigating evolutionary radiations. Bioinformatics 24:129-131.

Harmon L.J., Losos, J.B., Jonathan Davies, T., Gillespie, R.G., Gittleman, J.L., Bryan Jennings, W., Kozak, K.H., McPeek, M.A., Moreno-Roark, F., Near, T.J., and A. Purvis. 2010. Early bursts of body size and shape evolution are rare in comparative data. Evolution 64:2385-2396.

Hibbeler, R.C. 2007. *Mechanics of Materials*. Prentice Hall.

Humason, G.L. 1962. *Animal Tissue Techniques*. W.H. Freeman and Co.

Huxley, T.H. 1860. Darwin on the Origin of Species. Westminster Review 17:541-570.

Jablonski, D. 2017. Approaches to macroevolution: 1. General concepts and origin of variation. Evol. Biol. 44:427-450.

Jackson, S.M. 2012. *Gliding mammals of the world*. CSIRO Publishing.

Johnson-Murray, J.L. (1987). The comparative myology of the gliding membranes of Acrobates, Petauroides and Petaurus contrasted with the cutaneous myology of Hemibelideus and Pseudocheirus (Marsupialia, Phalangeridae) and with selected gliding Rodentia (Sciuridae and Anamoluridae). Aust. J. Zool. 35:101-113.

Kawashima, T., Thorington Jr, R.W., Bohaska, P.W., and F. Sato. 2017. Evolutionary transformation of the palmaris longus muscle in flying squirrels (Pteromyini: Sciuridae): an anatomical consideration of the origin of the uniquely specialized styliform cartilage. Anat. Rec. 300:340-352.

Kobayashi, M. 2017. Homology of the muscles within the uropatagium membrane in Leschenault's rousette (Rousettus leschenaultii). Z. Saugetierkd. 86:102-106.

Koyabu, D., and N.T. Son. 2014. Patterns of postcranial ossification and sequence heterochrony in bats: Life histories and developmental trade-offs. J. Exp. Zool. Part B. 322:607-618.

Kunz, T.H. and M.B. Fenton, eds. 2005. *Bat Ecology*. Univ. of Chicago Press.

López-Fernández, H., Arbour, J.H., Winemiller, K.O., and R.L. Honeycutt. 2013. Testing for ancient adaptive radiations in Neotropical cichlid fishes. Evolution 67:1321-1337.

Martill, D.M., Tischlinger, H., and N.R. Longrich. 2015. A four-legged snake from the Early Cretaceous of Gondwana. Science 349:416-419.

Meng, Q.J., Grossnickle, D.M., Liu, D., Zhang, Y.G., Neander, A.I., Ji, Q., and Z.X. Luo. 2017. New gliding mammaliaforms from the Jurassic. Nature 548:291-296.

Moczek, A.P. 2008. On the origins of novelty in development and evolution. BioEssays 30:432-447.

Müller, G.B., and G.P. Wagner. 1991. Novelty in evolution: restructuring the concept. Annu. Rev. Ecol. Syst. 22:229-256 (1991).

Müller, G.B. 2010. Epigenetic innovation. *Evolution: The extended synthesis*, 307-332.

Musser, J.M., Wagner, G.P., and R.O. Prum. 2015. Nuclear β-catenin localization supports homology of feathers, avian scutate scales, and alligator scales in early development. Evol. Dev. 17:185-194.

Novick, A., and B.A. Dale. 1971. Foraging behavior in fishing bats and their insectivorous relatives. J. Mammal. 52:817-818.

Orr, H.A., and J.A. Coyne. 1992. The genetics of adaptation: a reassessment. Am. Nat. 140:725-742.

Pennell, M.W., Eastman, J.M., Slater, G.J., Brown, J.W., Uyeda, J.C., FitzJohn, R.G., Alfaro, M.E., and L.J. Harmon. 2014. geiger v2.0: an expanded suite of methods for fitting macroevolution models to phylogenetic trees. Bioinformatics 30:2216-2218.

Pigliucci, M. 2008. What, if anything, is an evolutionary novelty? Philos. Sci. 75:887-898.

R Core Team. 2017. R: A language and environment for statistical computing.

Revell, L. J. 2009. Size-correction and principal components for interspecific comparative studies. Evolution 63:3258-3268.

Revell, L. J. 2010. Phylogenetic signal and linear regression on species data. Methods Ecol. Evol. 1:319-329.

Revell, L.J. 2012. phytools: An R package for phylogenetic comparative biology (and other things). Methods Ecol. Evol. 3:217-223.

Revell, L.J. 2013. Two new graphical methods for mapping trait evolution on phylogenies. Methods Ecol. Evol. 4:754-759.

Reyes-Amaya, N., Jerez, A., and D. Flores. 2017. Morphology and postnatal development of lower hindlimbs in Desmodus rotundus (Chiroptera: Phyllostomidae): a comparative study. Anat. Rec. 300:2150-2165.

Sarin, V.K., Erickson, G.M., Giori, N.J., Bergman, A.G., and D.R. Carter. 1999. Coincident development of sesamoid bones and clues to their evolution. Anat. Rec, 257:174-180.

Schutt, W.A., and N.B. Simmons. 1998. Morphology and homology of the chiropteran calcar, with comments on the phylogenetic relationships of Archaeopteropus. J. Mamm. Evol. 5:1-32.

Shi, J.J., and D.L. Rabosky. 2015. Speciation dynamics during the global radiation of extant bats. Evolution 69:1528-1545.

Shubin, N., Tabin, C., and S. Carroll. 2009. Deep homology and the origins of evolutionary novelty. Nature 457:818-823.

Simmons, N.B. 2005. Order Chiroptera. *Mammal Species of the World: A Taxonomic and Geographic Reference*. 312-529. Johns Hopkins Univ. Press.

Simmons, N.B., Seymour, K.L., Habersetzer, J., and G.F. Gunnell. 2008. Primitive Early Eocene bat from Wyoming and the evolution of flight and echolocation. Nature 451:818-821.

Simmons, N.B., and J.H. Geisler. 1998. Phylogenetic relationships of Icaronycteris, Archaeonycteris, Hassianycteris, and Palaeochiropteryx to extant bat lineages, with

comments on the evolution of echolocation and foraging strategies in Microchiroptera. B. Am. Mus. Nat. Hist. 235:1-182.

Simpson, G.G. 1944. *Tempo and mode in evolution*. Columbia Univ. Press.

Slater, G.J., Price, S.A., Santini, F., and M.A. Alfaro. 2010. Diversity vs disparity and the evolution of modern cetaceans. Proc. R Soc. Lond., B, Biol. Sci. 277:3097-3104.

Slater, G.J., and M.W. Pennell. 2013. Robust regression and posterior predictive simulation increase power to detect early bursts of trait evolution. Syst. Biol. 63:293-308.

Slater, G.J., and A.R. Friscia. 2019. Hierarchy in adaptive radiation: A case study using the Carnivora (Mammalia). Evolution 73:524-539.

Smith, T., Habersetzer, J., Simmons, N.B., and G.F. Gunnell. 2012. Systematics and paleobiogeography of early bats. *Evolutionary History of Bats: Fossils, Molecules and Morphology*. 23-66. Cambridge, Univ. Press.

Stanchak, K.E., and S.E. Santana. 2018. Assessment of the hindlimb membrane musculature of bats: Implications for active control of the calcar. Anat. Rec. 301, 441-448.

Storch, G., Sigé, B., and J. Habersetzer. 2002. Tachypteron franzeni n. gen., n. sp., earliest emballonurid bat from the Middle Eocene of Messel (Mammalia, Chiroptera). Palaeontol. Z. 76:189-199.

Teeling, E.C., Springer, M.S., Madsen, O., Bates, P., O'brien, S.J., and W.J. Murphy. 2005. A molecular phylogeny for bats illuminates biogeography and the fossil record. Science 307:580-584.

Vaughan, T.A. 1970. The skeletal system. *Biology of bats* v*1*, 98-139. Academic Press, NY.

Vickaryous, M.K., and W.M. Olson. 2007. Sesamoids and ossicles in the appendicular skeleton. *Fins into limbs: evolution, development and transformation*. Univ. Chicago Press.

Wagner, G.P. 2014. *Homology, genes, and evolutionary innovation*. Princeton Univ. Press.

Witton, M.P. 2013. *Pterosaurs: natural history, evolution, anatomy*. Princeton University Press.

Xu, X., Zheng, X., Sullivan, C., Wang, X., Xing, L., Wang, Y., Zhang, X., O'Connor, J.K., Zhang, F., and Y. Pan. 2015. A bizarre Jurassic maniraptoran theropod with preserved evidence of membranous wings. Nature 521:70-73.

SUPPORTING INFORMATION

Specimen List for scanning and histology with anatomical descriptions:

Institution Acronyms in List of Specimens:

AMNH: American Museum of Natural History Mammal Collection

FMNH: Field Museum of Natural History Mammal Collection

Lab: Santana Lab in the Department of Biology at the University of Washington

MCZ: Museum of Comparative Zoology Mammal Collection

MVZ: Museum of Vertebrate Zoology Mammal Collection

NMNH: United States National Museum Mammal Collection at the Smithsonian National Museum of Natural History

PSM: Slater Museum of Natural History Mammal Collection

UWBM: Burke Museum of Natural History and Culture Mammal Collection

CT scanning and histology specimen list with anatomical descriptions of calcar and ankle modifications. Note that, because of the limited number of individuals per species in our sample, we were unable to confirm absence of a synovial joint in the histological sections. This is because the soft tissues around the joint did not always remain intact during sectioning, or the section was not in the adequate orientation/position to capture the tissues forming the synovial capsule.

Artibeus jamaicensis (Phyllostomidae) – Santana Lab 022614-25

Procedures: CT scanning and histological sectioning.

Small calcified nodule of cartilaginous calcar near articulation with calcaneus. No evidence of internal structure (i.e., not bony). Synovial joint between calcar and calcaneus. Sesamoid on plantar side of tibia, just above astragalus.

Scanned on Skyscan1172 at 8.88μm, 59kV, 167μA.

Balantiopteryx plicata (Emballonuridae) – Santana Lab 0229-06

Procedures: CT scanning and histological sectioning.

Long calcified portion of calcar with less densely-calcified or uncalcified interior. Calcar is entirely cartilaginous. More densely calcified "cap" to calcar at articulation with calcaneus. Sesamoid on plantar/lateral side of outer cuneiform (the cuneiform above the 1st metatarsal).

Scanned on Skyscan1172 at 7.97μm, 59kV, 167μA.

Cynopterus brachyotis (Pteropodidae) – UWBM (pending); Lubee Bat Conservancy #929841.

Procedures: CT scanning, diceCT scanning, dissection, and histological sectioning.

Uncalcified cartilage calcar not contiguous with the tendon of the *m. gastrocnemius*. Sesamoid on plantar/lateral side of outer cuneiform.

Scanned on Skyscan1172 at 10.58μm, 49kV, 200μA. diceCT scan on Skyscan1172 at 10.58μm, 40kV, 250μA after 2 days in 3% (total solute) Lugol's iodine.

Desmodus rotundus (Phyllostomidae) – Santana Lab 022714-06

Procedures: CT scanning and histological sectioning.

Calcar has small, bony nodule with clear internal structure but is distally cartilaginous. Synovial joint between calcar and calcaneus. Middle cuneiform is contiguous with/fused to the navicular. Sesamoid on plantar side of outer cuneiform and the middle cuneiform/navicular fusion. Sesamoid on plantar side of proximal end of 5th metarsal.

Scanned on Skyscan1172 at 12.67μm, 59kV, 167μA.

Eptesicus fuscus (Vespertilionidae) – Santana Lab KES 037

Procedures: CT scanning and histological sectioning.

Cartilaginous calcar has lightly calcified section and an uncalcified "keel" hook. Synovial joint between calcar and calcaneus. Sesamoid on dorsal side of astragalus. Sesamoid on plantar/lateral side of outer cuneiform. Small nodule on plantar side of cuboid and under proximal end of calcar; these are possibly scan artefacts.

Scanned on Skyscan1172 at 11.11μm, 40kV, 250μA.

Furipterus horrens (Furipteridae) – AMNH 142903

Procedures: CT scanning (whole specimen).

Long, calcified cartilage calcar. Sesamoid above (superior to) outer cuneiform.

Scanned on Skyscan1173 at 12.14μm (only hindlimbs in scan), 70kV, 114μA.

Glossophaga longirostris (Phyllostomidae) – Santana Lab GR110

Procedures: CT scanning and histological sectioning.

Uncalcified, cartilaginous calcar. Sesamoid on plantar side of tibia and astragalus.

Scanned on Skyscan1172 at 9.93μm, 59kV, 167μA.

Hipposideros armiger (Hipposideridae) – AMNH 272276

Procedures: CT scanning and histological sectioning.

Uncalcified cartilaginous calcar (but with perhaps a slight calcified band just above calcaneus). Sesamoid on dorsal side of astragalus. Sesamoid on plantar/lateral side of outer cuneiform. Sesamoid on plantar side of proximal end of 5th metatarsal.

Scanned on Skyscan1172 at 9.80µm, 49kV, 200µA.

Macrotus waterhousii (Phyllostomidae) – Slater Museum FHA135

Procedures: CT scanning and histological sectioning.

Calcar is proximally bony. Sesamoid on plantar/lateral side of middle cuneiform. Lots of detritus in specimen that appears in scan.

Scanned on Skyscan1172 at 8.88µm, 59kV, 167µA.

Megaderma spasma (Megadermatidae) – FMNH 205388

Procedures: CT scanning and histological sectioning.

Uncalcified cartilaginous calcar (but with perhaps a slight calcified band just above calcaneus). Calcar forms synovial joint with calcaneus. Sesamoid on plantar/lateral side of outer cuneiform. Sesamoid on plantar side of proximal end of 5th metatarsal.

Scanned on Skyscan1172 at 9.80µm, 49kV, 200µA.

Molossus molossus (Molossidae) – Slater Museum FHA1857

Procedures: CT scanning and histological sectioning.

Calcified calcar with internal bony structure at proximal end; cartilage distally. Calcar forms synovial joint with calcaneus. Sesamoid on dorsal side of astragalus. Sesamoid on plantar/lateral side of outer cuneiform. Sesamoid on plantar side of middle and outer cuneiforms.

Scanned on Skyscan1172 at 10.71μm, 59kV, 167μA.

Myotis californicus (Vespertilionidae) – Santana Lab KES 026

Procedures: CT scanning and histological sectioning.

Calcified cartilage calcar that forms an uncalcified "keel" hook. Calcar forms synovial joint with calcaneus. Sesamoid on plantar/lateral side of outer cuneiform.

Scanned on Skyscan1172 at 10.71μm, 40kV, 250μA.

Mystacina tuberculata (Mystacinidae) – MVZ 173918

Procedures: CT scanning (whole specimen).

Calcified calcar with internal structure that appears bony at proximal end. Calcification forms two long "tines". Sesamoid on plantar/lateral side of outer cuneiform.

Scanned on Skyscan1173 at 20.96μm, 60kV, 133μA.

Natalus mexicanus (Natalidae) – Santana Lab 0229-02

Procedures: CT scanning and histological sectioning.

Calcified cartilage calcar with less densely-calcified or uncalcified interior. Medial and middle cuneiforms appear fused. Sesamoid on dorsal side of distal end of astragalus/proximal end of fused medial and middle cuneiforms.

Scanned on Skyscan1172 at 6.92μm, 59kV, 167μA.

Noctilio leporinus (Noctilionidae) – Slater Museum FHA1651

Procedures: CT scanning and histological sectioning.

Calcar has long calcified section that has distinctly bony internal structure, including what appear to be small trabeculae. Sesamoid on plantar side of outer and middle cuneiforms. Sesamoid on plantar side of proximal end of 5th metatarsal.

Scanned on Skyscan1172 at 12.15μm, 59kV, 167μA.

Nycteris hispida (Nycteridae) – USNM 478968

Procedures: CT scanning and histological sectioning.

Long, calcified cartilage calcar with less densely-calcified or uncalcified interior. Cuboid, medial cuneiform, and middle cuneiform are fused. Sesamoid on plantar side of outer cuneiform.

Scanned on Skyscan1172 at 6.88μm, 49kV, 200μA.

Pteronotus quadridens (Mormoopidae) – Slater Museum FHA 780

Procedures: CT scanning and histological sectioning.

Long, primarily calcified cartilage calcar with bony tissue at proximal end near articulation with calcaneus. Proximal cartilaginous portion of calcar has less-densely calcified interior. Sesamoid on plantar side of lateral outer cuneiform. Sesamoid on plantar side of proximal end of 5th metatarsal. Sesamoid on dorsal/medial side of cuboid.

Scanned on Skyscan1172 at 6.92μm, 59kV, 167μA.

Pteropus sp. (Pteropodidae) – Herring Lab #76.

Procedures: CT scanning, diceCT scanning, dissection.

Uncalcified cartilage calcar that is contiguous with the tendon of the *m. gastrocnemius* (based on dissection).

Scanned on Skyscan1172 at 26.44µm, 49kV, 200µA. diceCT scan on Skyscan1172 at 26.44µm, 40kV, 250µA after 3 days in 3% (total solute) Lugol's iodine.

Rhinolophus affinis (Rhinolophidae) – AMNH 234034

Procedures: CT scanning and histological sectioning.

Uncalcified cartilaginous calcar. Sesamoid on dorsal side of distal end of astragalus.

Scanned on Skyscan1172 at 6.40µm, 49kV, 200µA.

Rhinopoma hardwickii (Rhinopomatidae) – FMNH 123185

Procedures: CT scanning and histological sectioning.

Uncalcified cartilaginous calcar. Sesamoid on dorsal side of distal end of astragalus. Sesamoid on plantar side of navicular. Sesamoid on plantar side of proximal end of 5th metatarsal.

Scanned on Skyscan1172 at 7.45µm, 49kV, 200µA.

Rousettus aegyptiacus (Pteropodidae) – Herring Lab #224.

Procedures: CT scanning, diceCT scanning, dissection, and histological sectioning.

Uncalcified cartilage calcar that is contiguous with the tendon of the *m. gastrocnemius* (based on dissection). Sesamoid on plantar/lateral side of outer cuneiform. Small nodule on dorsal side of foot between proximal ends of calcaneus and astragalus. This small nodule does not appear to be present in the scan of the other foot.

Scanned on Skyscan1172 at 13.22µm (Lft – analyzed in Mimics) 10.45µm (Rft), 49kV, 200µA. diceCT scan (Rft) on Skyscan1172 at 10.18µm, 40kV, 250µA after 2 days in 3% (total solute) Lugol's iodine.

Thyroptera tricolor (Thyropteridae) – MVZ 158246

Procedures: CT scanning (whole specimen).

Long, primarily uncalcified cartilage calcar with calcified nodule at articulation with calcaneus. Calcar has two obvious uncalcified "keel"-like structures (based upon external examination of specimen). Navicular and middle cuneiform are fused. Sesamoid on plantar side of outer cuneiform.

Scanned on Skyscan1173 at 17.06µm , 60kV, 133µA.

Code for Evolutionary Modeling in R:

```
# Code for Stanchak et al. 2019 Evolution
# Most lines of codes are samples and need to be re-run
# with the proper data (e.g., nozeroData then noPterodata)
# The tree is from Shi & Rabosky (2015) Evolution.
# We updated taxon names in the Shi & Rabosky tree before analysis
# to match those in the data set supplied with our manscuript.

library(ape)
library(geiger)
library(phytools)
library(nlme)

# Read in Data; Define Data sets
ShiTree<-read.nexus(file="ShiRabosky_renamed.nex")
calcarData<-read.csv("CalcarAnat_Evolution_SuppInfoAnalysisData.csv", header=1,
row.names=4)
nozeroData <- calcarData[which(calcarData$Cal_mean > 0), ]
noPteroData <- calcarData[which(calcarData$Family != "Pteropodidae"), ]
nozeroPteroData <- noPteroData[which(noPteroData$Cal_mean > 0), ]
phylloData <- calcarData[which(calcarData$Family == "Phyllostomidae"),]

# Trim Tree

trimmed<-treedata(ShiTree, nozeroPteroData, sort=T)
trim.data<-trimmed$data
trim.tree<-trimmed$phy
name.check(trim.tree, trim.data)

# Ultrametric version of tree for OU analysis

bat.tree<-trim.tree
ntaxa<-Ntip(bat.tree)
dists<-dist.nodes(bat.tree)[(ntaxa+1),1:ntaxa]
for(i in 1:length(bat.tree$tip.label)){
  dis<-dists[i]
  a<-max(dists)-dis
  edges<-which(bat.tree$edge[,2]==i)
  bat.tree$edge.length[edges]<-bat.tree$edge.length[edges]+a
}

# Define vars

FA<-as.numeric(trim.data[,c("FA_mean")])
names(FA)<-rownames(trim.data)
```

```
Cal<-as.numeric(trim.data[,c("Cal_mean")])
names(Cal)<-row.names(trim.data)
Tib<-as.numeric(trim.data[,c("Tib_mean")])
names(Tib)<-row.names(trim.data)
CdT<-as.numeric(trim.data[,c("CdT_mean")])
names(CdT)<-row.names(trim.data)
CdF<-as.numeric(trim.data[,c("CdF_mean")])
names(CdF)<-row.names(trim.data)

# Define residuals

FAresid<-phyl.resid(trim.tree, FA, Cal, method="BM")
FAres<-FAresid$resid
Tibresid<-phyl.resid(trim.tree, Tib, Cal, method="BM")
Tibres<-Tibresid$resid


#### New MDI p function
.area.between.curves<-geiger:::.area.between.curves

getMDIp<-function (dttRes) {
  foo <- function(x) {
    return(.area.between.curves(x = dttRes$times, f1 = x,
                                f2 = dttRes$dtt))
  }
  mdis <- apply(dttRes$sim, 2, foo)
  pVal <- length(which(mdis >= 0))/length(mdis)
  return(pVal)
}

##### posterior predictive tests sensu Slater and Pennell - JHA

dtt.rescaled<-function (phy, data, index = c("avg.sq", "avg.manhattan", "num.states"),
                        mdi.range = c(0, 1), nsim = 0, CI = 0.95, plot = TRUE, calculateMDIp = F,
                        #adding a few model parameters in
                        model, scaler, rate)
{
  disp = match.arg(index, c("avg.sq", "avg.manhattan", "num.states"))

  #I moved this section up and based it on the unscaled tree so the times will be right
  ltt <- sort(branching.times(phy), decreasing = TRUE)
  ltt <- c(0, (max(ltt) - ltt)/max(ltt))

  #Now I am rescaling the tree so the simulations reflect different models
  if (model == "EB") phy<-rescale(phy,model=model,scaler)
```

```
  #Pulling this from our model values
  s <- as.matrix(rate)

  #Now the function follows mostly the same as the original
  td <- treedata(phy, data)
  dtt.data <- .dtt(td$phy, td$data, disp = disp)

  dtt.sims = NULL
  MDI = NULL
  ylim = c(range(pretty(dtt.data)))
  if (is.numeric(nsim)) {
    if (nsim > 0) {
      sims <- sim.char(td$phy, s, nsim)
      dtt.sims <- .dtt(td$phy, sims)
      mean.sims <- apply(dtt.sims, 1, mean)
      median.sims <- apply(dtt.sims, 1, median)
      MDI <- unname(.area.between.curves(ltt, apply(dtt.sims,
                                          1, median), dtt.data, sort(mdi.range)))
      names(MDI) = disp
      colnames(dtt.sims) = NULL
      yy = range(dtt.sims)
      ylim = range(c(ylim, yy))
    }
  }
  if (plot) {
    plot(ltt, dtt.data, xlab = "relative time", ylab = "disparity",
         ylim = ylim, bty = "n", type = "n")
    if (!is.null(dtt.sims)) {
      poly = .dtt.polygon(dtt.sims, ltt, alpha = 1 - CI)
      polygon(poly[, "x"], poly[, "y"], col = .transparency("lightgray",
                                            0.5), border = NA)
      lines(ltt, median.sims, lty = 2)
    }
    lines(ltt, dtt.data, type = "l", lwd = 2)
  }
  res = list(dtt = dtt.data, times = ltt, sim = dtt.sims, MDI = MDI)
  drp = sapply(res, function(x) is.null(x))
  if (any(drp))
    res = res[-which(drp)]
  if (calculateMDIp) {
    pVal <- getMDIp(res)
    res <- c(res, MDIpVal = pVal)
  }
  return(res)
}
```

```
# if needed:
par(mar=c(5, 4, 4, 2) + 0.1)

########### running the new DTT function
## and fitContinuous models
#loading a few internal functions
.dtt<-geiger:::.dtt
.area.between.curves<-geiger:::.area.between.curves
.dtt.polygon<-geiger:::.dtt.polygon
.transparency<-geiger:::.transparency

BMmodel <- fitContinuous(trim.tree, CdT, model="BM")
dttresBM <- dtt.rescaled(phy=trim.tree, CdT, nsim=1000, model="BM",
rate=BMmodel$opt$sigsq)
getMDIp(dttresBM)
EBmodel <- fitContinuous(trim.tree, CdT, model="EB")
dttresEB <- dtt.rescaled(phy=trim.tree, CdT,
nsim=1000,model="EB",scaler=EBmodel$opt$a,rate=EBmodel$opt$sigsq)
getMDIp(dttresEB)
OUmodel <- fitContinuous(bat.tree, CdT, model="OU")

BMmodel <- fitContinuous(trim.tree, CdF, model="BM")
dttresBM <- dtt.rescaled(phy=trim.tree, CdF, nsim=1000, model="BM",
rate=BMmodel$opt$sigsq)
getMDIp(dttresBM)
EBmodel <- fitContinuous(trim.tree, CdF, model="EB")
dttresEB <- dtt.rescaled(phy=trim.tree, CdF,
nsim=1000,model="EB",scaler=EBmodel$opt$a,rate=EBmodel$opt$sigsq)
getMDIp(dttresEB)
OUmodel <- fitContinuous(bat.tree, CdF, model="OU")

BMmodel <- fitContinuous(trim.tree, Tibres, model="BM")
dttresBM <- dtt.rescaled(phy=trim.tree, Tibres, nsim=1000, model="BM",
rate=BMmodel$opt$sigsq)
getMDIp(dttresBM)
EBmodel <- fitContinuous(trim.tree, Tibres, model="EB")
dttresEB <- dtt.rescaled(phy=trim.tree, Tibres,
nsim=1000,model="EB",scaler=EBmodel$opt$a,rate=EBmodel$opt$sigsq)
getMDIp(dttresEB)
OUmodel <- fitContinuous(bat.tree, Tibres, model="OU")

BMmodel <- fitContinuous(trim.tree, FAres, model="BM")
dttresBM <- dtt.rescaled(phy=trim.tree, FAres, nsim=1000, model="BM",
rate=BMmodel$opt$sigsq)
getMDIp(dttresBM)
EBmodel <- fitContinuous(trim.tree, FAres, model="EB")
```

```
dttresEB <- dtt.rescaled(phy=trim.tree, FAres,
nsim=1000,model="EB",scaler=EBmodel$opt$a,rate=EBmodel$opt$sigsq)
getMDIp(dttresEB)
OUmodel <- fitContinuous(bat.tree, FAres, model="OU")

# Akaike weights
AIC.scores <- c(1010.446268, 1010.176096, 1012.511127)
names(AIC.scores) <- c("BM", "EB", "OU")
aicw(AIC.scores)


# plot contMap

length.contmap<-contMap(trim.tree, CdT, type="fan", ftype="off")
n<-length(length.contmap$cols)
#rampfxn<-colorRampPalette(c(rgb(1,1,1),rgb(0,0,0)))
#neonramp<-colorRampPalette(c(rgb(0.95,0,0.5), rgb(0.75,0.75,0.75), rgb(0,0.95,0.1)))
pinkramp<-colorRampPalette(c(rgb(0,0,0), rgb(0.80,0,0.5), rgb(1,1,1)))
length.contmap$cols[]<-pinkramp(n)
length.contmap<-setMap(length.contmap, invert=T)
plot(length.contmap, type="fan", fsize=0.3, legend=T, ftype="off")
```

CHAPTER 3

Motion of the calcar during flight in *Carollia perspicillata* (Phyllostomidae: Chiroptera)

Authors:

Kathryn E. Stanchak[1*], David B. Boerma[2], Sharlene E. Santana[1], Sharon M. Swartz[2]

[1]Department of Biology, University of Washington, Seattle, WA 98103 USA and Department of Mammalogy, Burke Museum of Natural History and Culture, Seattle, WA 98103 USA.

[2]Department of Ecology and Evolutionary Biology, Brown University, Providence, RI, 02906, USA.

ABSTRACT

Bat wings exhibit many anatomical modifications that allow them to fly, including elongated forearms and a series of membranes that span their limbs. One particularly enigmatic feature of bat wings is the calcar, a novel skeletal element that projects from the ankle into the hindlimb membrane. Although the anatomy of the calcar has been studied in detail, existing hypotheses of calcar function are nonspecific and based only on observations. Here, we provide the first quantitative study of calcar function with a kinematic analysis of calcar motion. The anatomy of the calcar suggests that it is able to rotate about its joint with the bat ankle. We used high speed videography to test whether and how the calcar of *Carollia perspicillata* (Phyllostomidae, Chiroptera) rotates relative to the other hindlimb elements in free, forward flight. We found that the calcar does exhibit rotation and that this rotation is greater in the vertical plane of motion than in a horizontal plane. Based on our results, we suggest that the calcar musculature may act to stabilize the calcar in the horizontal plane, leaving it free to rotate in the vertical plane as needed during the flight stroke.

ABBREVIATIONS

AngleCAK: the angle formed by the vector between the ankle and the tip of the calcar and the vector between the ankle and the knee.

AngleC_AKH: the angle formed by the vector between the ankle and the foot and the vector between the ankle and the knee.

INTRODUCTION

Flying animals exhibit many morphological features that enable them to take to the air. Insect wings are paired extensions of their exoskeleton that are stiffened by intersecting veins. Bird wings consist of heavily-modified forelimb skeletons and feathers that project from their forelimb integument. Bats also have a highly-modified forelimb skeleton, but their wings consist of a thin integumentary membrane that spans both the fore- and hindlimbs. Unlike relatively stiff chitinized insect wings or keratinized bird feathers, bat membranes are highly compliant, which presents functional challenges for generating lift and thrust. Bats have many anatomical features within their membranes that may help them stiffen or relax the membrane structure when necessary during the flight stroke. These include bundles of collagen and elastin fibers and cutaneous muscles (Holbrook and Odland, 1978; Cheney et al., 2015; Cheney et al., 2017) as well as skeletal elements that pass through the membrane (Norberg, 1972). Because the skeletal elements for the bat limbs can move relative to each other, they can expand and contract the membrane and therefore alter the surface area and shape of the wing.

The bat hindlimb contains one skeletal element not found in the hindlimbs of non-flying mammals: the calcar. The bat calcar is a rod-shaped, cartilaginous or bony element in the bat ankle that articulates with the calcaneus ankle bone (Fig. 1; Schutt and Simmons, 1998; Stanchak

et al., 2019). In many species, the articulation between the calcar and the calcaneus forms a synovial joint, suggesting that there is relative motion between the two skeletal elements (Stanchak et al. 2019). Manual manipulation of the calcar in deceased bat individuals also suggests that the calcar is mobile about this joint. There are skeletal muscles that insert on the calcar: a depressor muscle (*m. depressor ossis styliformis*) that might act in contraction to rotate the calcar about its joint with the calcaneus, pulling the calcar away from the body and spreading the hindlimb membrane; and a muscle that runs through the hindlimb membrane that might act in contraction to pull the calcar towards the body (*m. calcaneocutaneus*; Schutt and Simmons, 1998; Stanchak and Santana, 2018). These muscles also suggest relative motion between the calcar and the other limb elements.

Bat hindlimbs are functionally important for locomotion. In all bats, hindlimbs are critical for landing in a roosting position (Riskin et al., 2005; Boerma et al., 2019) and, in many species, for catching prey (Altenbach, 1989; Fenton and Bogdanowicz, 2002). Some bats commonly use quadrupedal locomotion, which explicitly requires use of the hindlimbs as well as the forelimbs (Riskin et al., 2006). The role of hindlimbs in bat flight is less clear. Experiments using a physical model of a bat in a wind tunnel suggested that the hindlimb membrane may be important for flight control (Gardiner et al., 2011). Flight trials of *Cynopterus brachyotis* (Pteropodidae) indicated that hindlimb motion during the flight stroke is not simply a consequence of wing membrane tension; rather, it is either active or a result of inertial effects (Cheney et al., 2014). Hindlimb motion in flight may vary among bat species. Four species in the family Vespertilionidae were found to exhibit exaggerated hindlimb motion during horizontal takeoffs, although similar motions were not observed in the phyllostomid bat *Carollia perspicillata* (Adams et al., 2012).

In this study, we investigated the motion of the calcar in Seba's short-tailed fruit bat (*Carollia perspicillata*, Phyllostomidae), a relatively abundant neotropical bat species that is commonly used as a model system for captive studies of bat flight, neurobiology, reproduction and development. Our goal was to understand if and how the calcar might rotate about its joint with the calcaneus. *C. perspicillata* forages for fruit, often by hovering or briefly landing near the fruit and then removing it with either the feet or mouth. Phyllostomid flight in general is considered "moderately fast and highly maneuverable" (Fleming, 1988), although we note that frugivorous bats in general have less demanding maneuverability requirements than bats foraging for mobile prey (Vaughan, 1970; see also Stanchak and Santana, 2018). We completed an anatomical analysis of a *C. perspicillata* foot to better understand and predict how the anatomy of the calcar-calcaneus joint and the calcar musculature might influence calcar motion. We then evaluated the motion of the calcar relative to the other hindlimb elements in free forward-flying *C. perspicillata* individuals.

MATERIALS AND METHODS

Assessment of Joint Anatomy

We investigated the gross anatomy of the ankles of one *C. perspicillata* specimen to assess the joint between the calcar and the calcaneus and the musculature associated with the calcar. We used diffusible iodine-based contrast-enhanced CT (diceCT, Gignac et al., 2016) scanning to image one foot (3% w/v Lugol's iodine for approximately 2 days; SkyScan 1172 μCT scanner, Bruker, Billerica, MA, USA) and histologically sectioned and stained the other ankle (8 μm paraffin sections, hematoxylin-eosin stain) of the same specimen. We examined the μCT scans using the visualization software DataViewer and CTVox (Bruker), and we

photographed the histological sections with an AmScope MU300 camera. The *C. perspicillata* specimen was collected from the island of Trinidad by KES; collection was approved the University of Washington IACUC (PROTO201700058) and conducted with all appropriate permits.

Flight Trials

To assess the motion of the calcar around its joint with the calcaneus, we performed forward-flight trials of five *C. perspicillata* individuals (4 to 6 trials per individual; 3 male, 2 female; mass of 18.5 – 21.5 g) from a colony kept in the Department of Ecology and Evolutionary Biology at Brown University. The trials took place in a flight corridor split into two partitions separated by a window. The bats flew from one side of the corridor through the window and within the view of a synchronized array of three high speed cameras (Phantom Miro 340, Vision Research, Wayne, NJ, USA; 800 frames per second; 200 μs exposure; Sigma DC 17-50mm 1:28 EX HSM lenses). The window was adjustable so that it could be sized to constrain the bat's flight path in view of the cameras yet remain wide enough to not inhibit the flight stroke. The bats either flew through the window on their own or were released from behind the window, but in the latter case the bats passed through the window and under the cameras after their initial takeoff. A sample video of a flight trial is provided in the electronic supplementary information. Prior to the beginning of an experimental session, we recorded calibration images using and 8 x 6 checkerboard of 20 nm squares. We used a white paint pen to mark hindlimb joints (tip of the calcar, foot, ankle, knee, and proximal femur near hip), a body point on the lumbar spine, and both wingtips. We also marked other anatomical locations that were not used in this study. The experimental protocol was approved by the Brown University IACUC.

Marker Tracking

We used the open-source video calibration and marker tracking software XMALab v.1.5.3 (Knörlein et al., 2016) to process and analyze flight trial videos. Using the associated checkerboard images and XMALab, we calibrated each video trial and optimized each calibration while applying the light-camera distortion model provided in XMALab. Then, one person (KES) manually tracked the position of the markers placed on the right hindlimb, which were the most visible in all trials. We only considered frames for further analysis if the marker placed at the tip of the calcar had a reprojection error of less than two pixels, as indicated by the XMALAb software. Because the position of the bats relative to the camera array changes within and across trials, this reprojection error does not directly translate to measurement error; we chose a value of two based on inspection during marker tracking. For all frames in which we were able to track a marker in at least two cameras, we exported the 3D positions of the marker. To document the wingbeat cycle, we tracked the left and right wingtips and exported the distance between these two markers. We also tracked the position of the body marker at the beginning and end of the portion of the trial for which the calcar reprojection error was satisfactory; these two body positions were used to calculate the average speed of the bat over the trial and the rise angle of the bat relative to the ground. To assess the marker tracking error, we exported the distance between the knee and hip markers and the distance between the knee and ankle markers for all frames included in a trial. We then calculated the standard deviations of these distances within a trial and across all trials for a particular individual. Because these markers are on rigid skeletal elements, the standard deviations of these distances both within and across trials should be low. All calculations were done in R v.3.6.0 (R Core Team, 2019).

Relative Position Calculations

As measures of whether and how the calcar moved throughout the wingbeat cycle, we considered the angles formed between the calcar and other hindlimb elements. The first angle we calculated is that formed by the vector from the ankle to the calcar tip and the vector from the ankle to the knee (AngleCAK; Fig. 2). This angle defines how the calcar might move two-dimensionally within the plane defined by the calcar and the tibia. It approximately describes motion within a horizontal, antero-posterior plane. An AngleCAK greater than 90° indicates a calcar rotated toward the foot, while an angle less than 90° indicates a calcar rotated toward the tibia. The second angle we considered is that between the vector from the ankle to the calcar tip and the plane defined by the triangle formed by the ankle, knee, and hip (AngleC_AKH; Fig. 2). This angle indicates a three-dimensional motion of the calcar relative to the movements of the leg, which is approximately motion within a transverse, dorso-ventral plane (approximately vertical as opposed to horizontal. We defined AngleC_AKH such that a negative angle indicates a calcar pointing out-of-plane ventrally, while a positive angle indicates a calcar pointing dorsally. These two angles together capture all rotation of the calcar about its joint with the calcaneus. We calculated these angles for all frames in which the required markers were trackable. We also calculated the range (maximum-minimum) of both angles for all trials. All calculations were done in R v.3.6.0 (R Core Team 2019). All R code for calculations is provided in the Supporting Information at the end of the chapter. Data files have been submitted as electronic Supporting Files with the dissertation.

Data Visualization – Wingbeat Cycle

For each flight trial, we plotted relative calcar angles as a function of percent wingbeat. To determine the wingbeat percentage of each frame in a trial, we counted the number of frames over the duration of a wingbeat, then rescaled the frames from the start of the upstroke to the end of the downstroke from 0 to 100. We considered the upstroke to begin in the frame in which the distance between the wingtips was at a minimum, when the bat had just completed a downstroke.

RESULTS

Calcar Anatomy

Histological sectioning revealed a synovial cavity at the joint between the calcar and the calcaneus in *C. perspicillata* as well as the *m. calcaneocutaneus*. Both the diceCT scan and histological sections revealed an *m. depressor ossis styliformis* that originates on the fifth metatarsal. In the diceCT scan, it is apparent that the *m. depressor ossis styliformis* inserts along the posterior margin of the calcar. This insertion does not extend all the way to the tip of the calcar; rather, it is only on the middle portion of the calcar's posterior margin (Fig. 1).

Relative Calcar Position

Marker tracking was consistent both across frames within individual trials and across trials, as evidenced by low standard deviations of the distance between the knee and the ankle markers and the distance between the hip and knee markers (Supplementary Table 1). During the upstroke, *C. perspicillata* adducts its hindlimbs and raises its wings such that they obscure its dorsum, which unfortunately often caused the tip of the calcar to be out of the view of the camera array (approximately 20-40% of the wingbeat as plotted in Figs. 3 and 4). However, the

trials for which we did obtain data in this wingbeat range did not suggest unobserved large motions of the calcar. In addition, usable frame data for most trials did not extend over a full wingbeat. Nonetheless, we compare the range of motion of the calcar in the trials as a basis for comparison of the two calcar angles.

The range of AngleCAK exhibited within a trial varied from 2.7° to 12.7°. The mean range of motion of AngleCAK exhibited within a trial was 7.2° (median 6.8°; Fig. 3). For two individuals (D, E), AngleCAK appeared to increase slightly during the downstroke before decreasing prior to the upstroke, but this was not the case for individual C, while the pattern for individuals A and B was unclear (Fig. 3).

AngleC_AKH exhibited a consistently higher range of motion than AngleCAK. AngleC_AKH varied from 12.7° to 51.8° across trials. The mean range of motion of AngleC_AKH was 32.5° (median 31.8°; Fig. 4). AngleC_AKH generally appeared to decrease as the upstroke progressed before increasing again during the downstroke,

All bats flew relatively slowly, between 2.21 and 3.86 m/s. Only one individual, “B”, flew at consistently highly speeds (4/5 trials above 3 m/s). However, because all of the other bats flew at relatively similar speeds, we did not observe any trend between flight speed and either AngleCAK or AngleC_AKH. We also did not observe any trend between rise angle and either angle.

DISCUSSION

The anatomy of the calcar of *C. perspicillata* implies that it can rotate about its joint with the calcaneus (as indicated by the presence of a synovial joint), perhaps actuated posteriorly by its prominent depressor muscle or anteriorly by the sheet-like cutaneous muscle. However, the

insertions of the calcar muscles along margins of the calcar rather than at the distal tip suggest that they act to stabilize the calcar rather than initiate large motions. This muscular anatomy is similar to that found in other primarily frugivorous phyllostomid bats that also have relatively short calcars (e.g., *Artibeus jamaicensis*; Stanchak and Santana, 2018; Stanchak et al., 2019). For both measured angles, we calculated ranges of motion greater than zero, demonstrating that the calcar does rotate during the wingbeat cycle. The range of AngleC_AKH was greater than that for AngleCAK, suggesting the calcar rotates more in the vertical dorsal-ventral plane than in the horizontal antero-posterior.

The decrease in AngleC_AKH occurred in the part of the upstroke when the bat's legs adduct and the calcar rotates ventrally so that the feet meet. This calcar movement may be caused by both rotation about the calcar-calcaneus joint as well as hip rotation that could not be resolved with our external markers. Large movements of the calcar in the primarily dorsal-ventral plane—as measured by AngleC_AKH—may be a result of moving the calcar out of the way for the upstroke and then repositioning the calcar so that it can support the hindlimb membrane when it is fully extended. Not all bat species adduct their legs so markedly during the wingbeat cycle (authors' observations), and it is unclear exactly what role this particular movement might play in the flight stroke.

Although AngleCAK varied among individuals, it stayed relatively constant throughout the wingbeat cycle. This might indicate that the absolute position of the calcar in this plane of action relative to the tibia is not critical for flight and is subject to inter-individual behavioral variation, so long as it remains stable with some unknown range. It is unclear if this angle is actively or passively maintained throughout the wingbeat cycle. The calcar muscle insertions along the margins of the calcar may act isometrically to keep the calcar stationary.

Because the foot and the calcar are connected through the *m. depressor ossis styliformis*, movement of the foot could cause movement of the calcar relative to the rest of the hindlimb. The calcar is also connected to the rest of the body through the hindlimb membrane, which may oppose the force on the calcar provided by movement of the foot. In addition, the *m. depressor ossis styliformis* may act in concentric contraction within this plane, actively pulling the calcar towards the foot despite the motion of the foot. Disentangling the roles of these three forces (pulling of the foot, contraction of the calcar muscles, and tension from the hindlimb membrane) would be a useful program for future research on calcar motion.

Whether or not the hindlimbs are critical for modulating flight parameters such as speed remains unclear. Cheney et al. (2014) did not find a relationship between the amplitude of ankle motion and flight speed. Although we recorded speed and rise angle for all flight trials, we did not observe any trend between these flight characteristics and our calcar motion measurements. Most of the bats in our experiments flew at similar speeds except one that flew at elevated speeds. This individual also had the greatest AngleCAK. Although we attempted to mark the joint positions consistently across individuals, it is possible that some variation in the marking led to variation in AngleCAK among individuals (although we note that we did not observe such distinction among individuals in AngleC_AKH). A follow-up investigation of calcar motion in bats might consider experimentally controlling flight speed in a wind tunnel set up to further investigate this potential relationship. A wind tunnel experimental set up would also remove any possible effects of rise angle on measurements of calcar motion.

Bats are highly ecologically diverse, and different species use their hindlimbs and hindlimb membranes differently. Consequently, calcar motion may be more or less pronounced among different bat species. For instance, some bats have long, calcified or body calcars and

feed on prey that present more of a functional challenge than stationary fruit. In some bats, the hindlimb membranes are directly implicated in prey capture, such as scooping insects in air or even fishing from the water surface with their feet. In these bats, the calcar may play more of an active role in flight and/or prey capture than in *C. perspicillata*. A comparative study of calcar motion among several ecologically variable bat species may be useful for discerning calcar function. In addition, similar membrane-associated rod-like structures have been found in a wide variety of vertebrates with membrane (summarized in Stanchak et al., 2019). A broader, comparative study of calcar function—including both kinematic and physiological studies—may help illuminate the role these structures have played in the evolution of flying and gliding vertebrates.

ACKNOWLEDGEMENTS

The Washington Research Foundation / Benjamin Hall Fellowship from the University of Washington Department of Biology provided funding for KES to visit the Aeromechanics and Evolutionary Morphology Lab of SMS at Brown University to conduct the bat behavioral experiments. Erika Tavares helped KES administratively during the visit as well as with animal care throughout the experiment. Sascha Morris and Isabel Young helped KES and DBB conduct the behavioral experiments.

FIGURES

Figure 1. Anatomy of the calcar in *C. perspicillata*. (A) 3D rendered image of lower hindlimb contrast-enhanced CT scan (see main text for methods), rendered in CTVox (Bruker). (B) Hematoxylin and eosin stained histological section of joint between calcar and calcaneus (see main text for methods). c, calcar; cs, calcaneus; mc, *m. calcaneocutaneus*; md, *m. depressor ossis styliformis*.

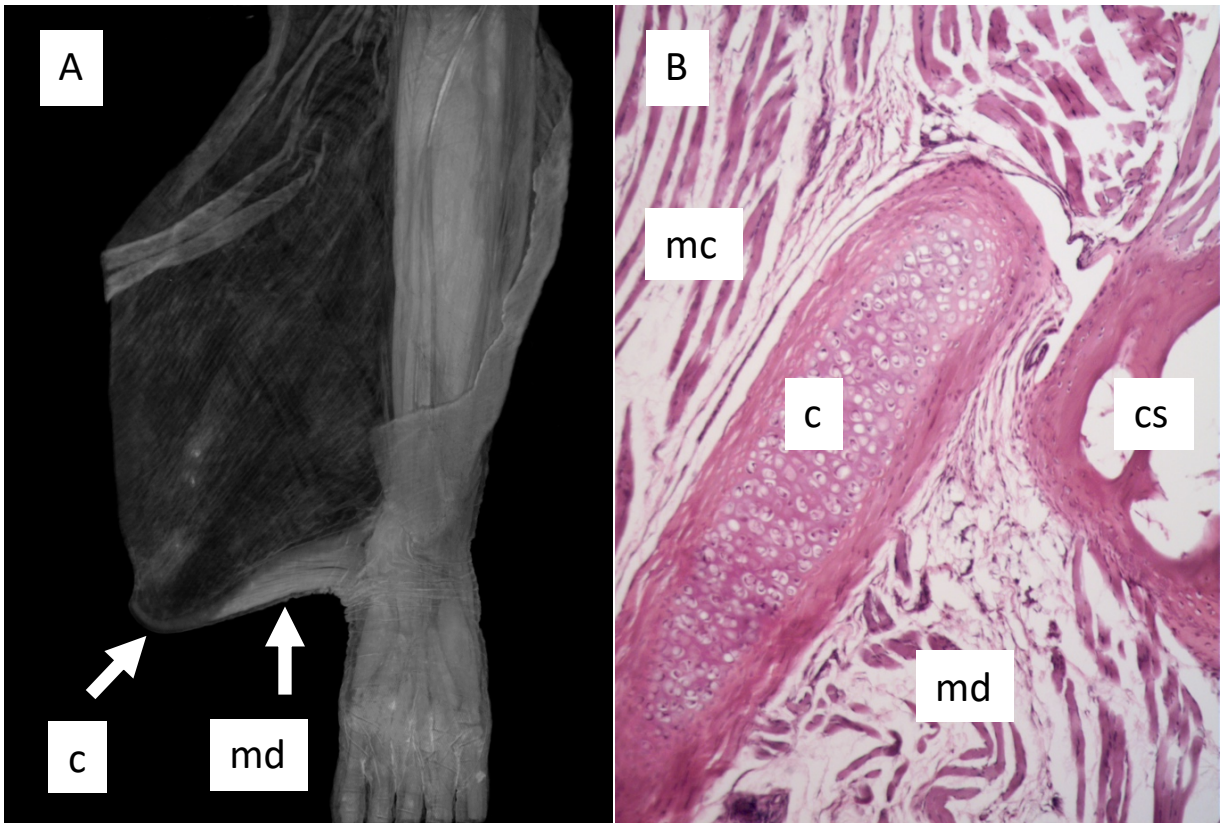

Figure 2. Diagram of lower *C. perspicillata* hindlimb demonstrating the two angles calculated from the flight trial videos. AngleCAK is formed by the vector from the ankle to the calcar tip and the vector from the ankle to the knee, while AngleC_AKH is that that between the vector from the ankle to the calcar tip and the plane defined by the triangle formed by the ankle, knee, and hip.

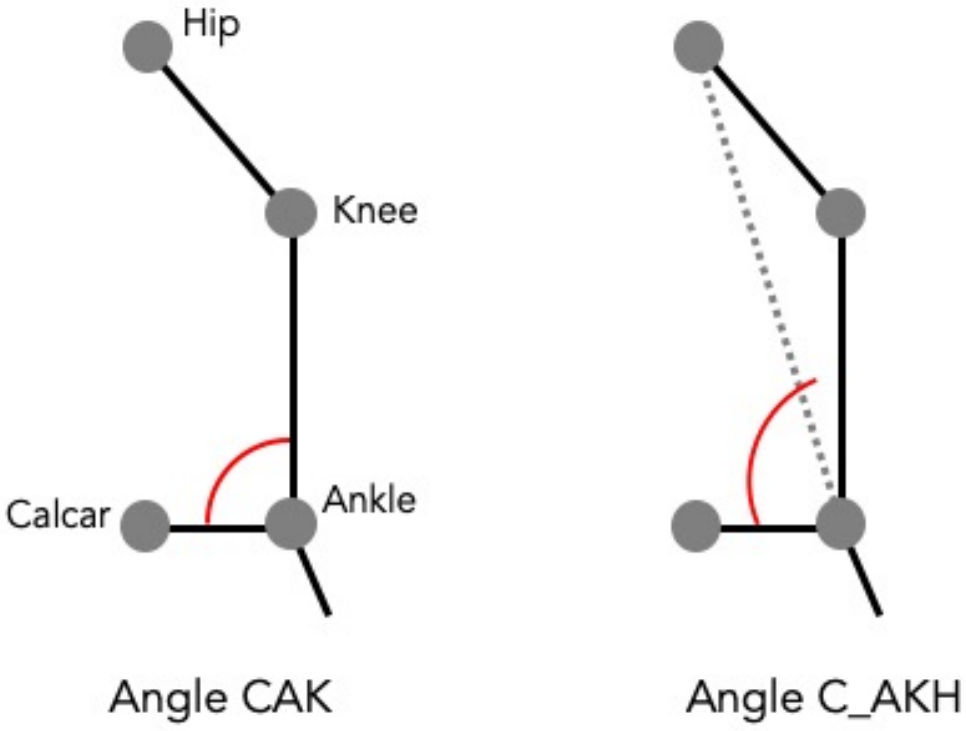

Figure 3. Angle between the calcar and the tibia (AngleCAK) plotted as a function of the wingbeat cycle for 4-6 trials each of 5 bat individuals.

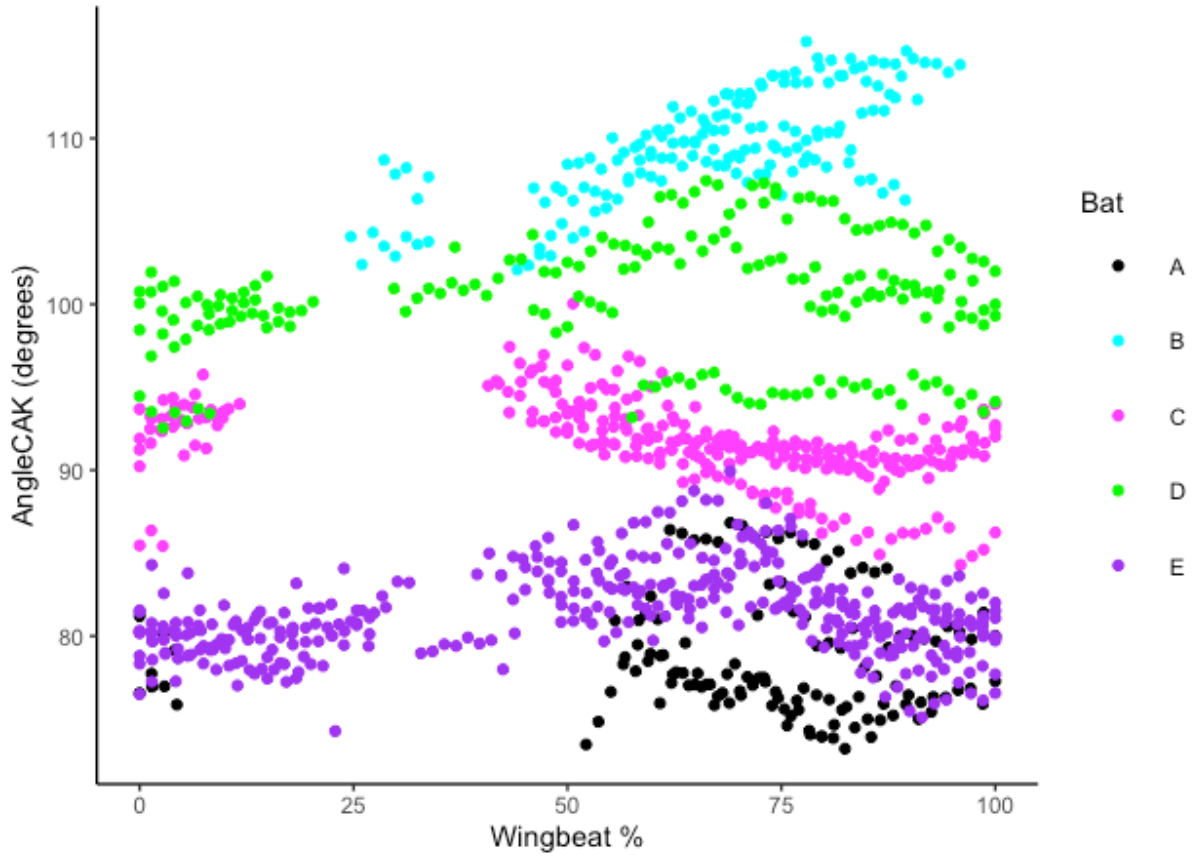

Figure 4. Angle between the calcar and the plane formed by the ankle, knee, and hip (AngleC_AKH) plotted as a function of the wingbeat cycle for 4-6 trials each of 5 bat individuals.

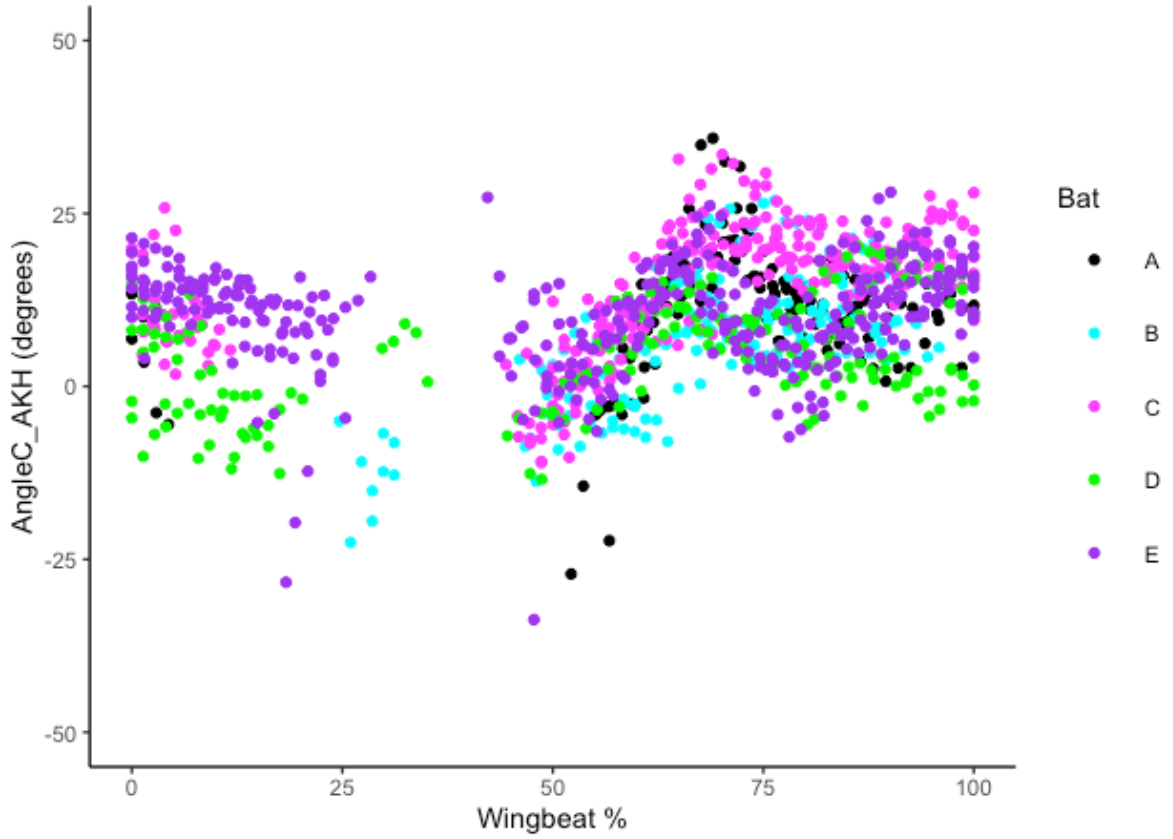

REFERENCES

Adams, R.A., Snode, E.R. and Shaw, J.R. (2012). Flapping tail membrane in bats produces potentially important thrust during horizontal takeoffs and very slow flight. *PLoS ONE*. 7, e32074.

Altenbach, J.S. (1989). Prey capture by the fishing bats *Noctilio leporinus* and *Myotis vivesi*. J. Mammal. 70, 421-424.

Boerma, D.B., Barrantes, J.P., Chung, C., Chaverri, G., and Swartz, S.M. (2019). Specialized landing maneuvers in Spix's disk-winged bats (*Thyroptera tricolor*) reveal linkage between roosting ecology and landing biomechanics. *J. Exp. Biol. pending issue*.

Cheney, J.A., Ton, D., Konow, N., Riskin, D.K., Breuer, K.S. and Swartz, S.M. (2014). Hindlimb motion during steady flight of the Lesser Dog-Faced Fruit Bat, *Cynopterus brachyotis*. *PLoS ONE*. 9, e98093.

Cheney, J.A., Konow, N., Bearnot, A. and Swartz, S.M. (2015). A wrinkle in flight: the role of elastin fibres in the mechanical behavior of bat wing membranes. *J. Roy. Soc. Interface*. 12, 20141286.

Cheney, J.A., Allen, J.J. and Swartz, S.M. (2017). Diversity in the organization of elastin bundles and intramembranous muscles in bat wings. *J. Anat*. 230, 510-523.

Fenton, M.B. and Bogdanowicz, W. (2002) Relationships between external morphology and foraging behavior. *Can. J. Zool.* 80, 1004-1013.

Fleming, T.H. (1988). The Short-tailed Fruit Bat: A Study in Plant-Animal Interactions. The University of Chicago Press, Chicago.

Gardiner, J.D., Dimitriadis, G., Codd, J.R. and Nudds, R.L. (2011). A potential role for bat tail membranes in flight control. *PLoS ONE*. 6, e18214.

Gignac, P.M., Kley, N.J., Clarke, J.A., Colbert, M.W., Morhardt, A.C., Cerio, D., Cost, I.N., Cox, P.G., Daza, J.D., Early, C.M. and Echols, M.S. (2016). Diffusible iodine-based contrast-enhanced computed tomography (diceCT): an emerging tool for rapid, high-resolution, 3-D imaging of metazoan soft tissues. *J. Anat*. 228, 889-909.

Holbrook, K.A. and Odland, G.F. (1978). A collagen and elastic network in the wing of the bat. *J. Anat*. 126, 2-36.

Knörlein, B.J., Baier, D.B., Gatesy, S.M., Laurence-Chasen, J.D. and Brainerd, E.L. (2016). Validation of XMALab software for marker-based XROMM. *J. Exp. Biol.* 219, 3701-3711.

Norberg, U.M. (1972). Bat wing structures important for aerodynamics and rigidity (Mammalia, Chiroptera). *Zeitschrift für Morphologie der Tiere*. 73, 45-61.

Riskin, D.K., Parsons, S., Schutt, Jr., W.A., Carter, G.G., and Hermanson, J.W. Terrestrial locomotion of the New Zealand short-tailed bat *Mystacina tuberculate* and the common vampire bat *Desmodus rotundus*. *J. Exp. Biol.* 209, 1725-1736.

Riskin, D.K., Bahlman, J.W., Hubel, T.Y., Ratcliffe, J.M., Kunz, T.H., and Swartz, S.M. (2009). Bats go head-under-heels: the biomechanics of landing on a ceiling. *J. Exp. Biol.* 7, 945-953.

Schutt, W.A. and Simmons, N.B. (1998). Morphology and homology of the chiropteran calcar, with comments on the phylogenetic relationships of *Archaeopteropus*. *J. Mamm. Evol.* 5, 1-32.

Stanchak, K.E. and Santana, S.E. (2018). Assessment of the hindlimb membrane musculature of bats: implications for active control of the calcar. *Anat. Rec.* 301, 441-448.

Stanchak, K.E., Arbour, J.H. and Santana, S.E. (2019). Anatomical diversification of a skeletal novelty in bat feet. *Evolution*. 73, 1591-1603.

Vaughan TA. (1970). Flight patterns and aerodynamics, In: Wimsatt WA, editor. Biology of Bats Vol. 1. New York: Academic Press. pp 195-216.

SUPPORTING INFORMATION

Supplementary Table 1.

Error statistics for marker tracking in flight trials. For every frame included in our analysis for each trial, we calculated the distance between the knee and the ankle as well as between the hip and the knee. Low variation of these distances within a trial and across all trials for each individual indicate low error in marker tracking.

Bat	Trial	Distance between knee and ankle (mm) (mean; standard deviation)	Distance between hip and knee (mm) (mean; standard deviation)
A	1	1.798; 0.014	0.612; 0.017
A	2	1.781; 0.012	0.621; 0.018
A	3	1.795; 0.020	0.625; 0.018
A	4	1.783; 0.017	0.637; 0.023
A	5	1.801; 0.016	0.627; 0.015
B	1	1.883; 0.012	0.659; 0.020
B	2	1.848; 0.011	0.669; 0.014
B	3	1.840; 0.014	0.617; 0.023
B	4	1.838; 0.012	0.641; 0.024
B	5	1.876; 0.008	0.694; 0.017
C	1	1.794; 0.012	0.623; 0.022
C	2	1.802; 0.014	0.625; 0.018
C	3	1.785; 0.016	0.634; 0.024
C	4	1.798; 0.013	0.613; 0.014
C	5	1.802; 0.015	0.623; 0.025

D	1	1.741; 0.008	0.683; 0.013
D	2	1.744; 0.015	0.654; 0.017
D	3	1.746; 0.013	0.672; 0.017
D	4	1.722; 0.015	0.660; 0.016
E	1	1.674; 0.016	0.941; 0.029
E	2	1.652; 0.016	0.918; 0.021
E	3	1.675; 0.015	0.913; 0.034
E	4	1.658; 0.019	0.917; 0.014
E	5	1.666; 0.023	0.917; 0.018
E	6	1.652; 0.029	0.905; 0.018

Code for calculations performed in R:

```
# Generate Speed and Rise Angle data for trials:
speedData <- read.csv("SpeedData.csv", header = T)
SpeedRiseData <- SpeedData(speedData)

# Calculate Angles, summary stats and Error estimates
kinematicData <- read.csv("KinematicData.csv", header=T)
angleData <- CalcarAngles(kinematicData)
summaryData <- AngleSummary(angleData)
errorData <- ErrorSummary(kinematicData)

# Merge Angle summary stats and speed/rise data for plotting
rownames(summaryData) <- as.factor(summaryData$BatTrial)
rownames(SpeedRiseData) <- as.factor(SpeedRiseData$BatTrial)
SummarySpeedData <- merge(summaryData, SpeedRiseData)
##########################################
# Generate summary statistics and errors
##########################################
AngleSummary <- function(data){
  Trials <- split(data, as.factor(data$BatTrial))
  x = length(Trials)
  summary <- data.frame()
  for (i in 1:x){
    CAKsd <- sd(as.numeric(as.vector(Trials[[i]]$angleCAK)), na.rm=TRUE)
    CAKmean <- mean(as.numeric(as.vector(Trials[[i]]$angleCAK)), na.rm=TRUE)
    CAKmax <- max(as.numeric(as.vector(Trials[[i]]$angleCAK)), na.rm=TRUE)
    CAKmin <- min(as.numeric(as.vector(Trials[[i]]$angleCAK)), na.rm=TRUE)
    CAKrange <- CAKmax - CAKmin
```

```
  C_AKHsd <- sd(as.numeric(as.vector(Trials[[i]]$angleC_AKH)), na.rm=TRUE)
  C_AKHmean <- mean(as.numeric(as.vector(Trials[[i]]$angleC_AKH)), na.rm=TRUE)
  C_AKHmax <- max(as.numeric(as.vector(Trials[[i]]$angleC_AKH)), na.rm=TRUE)
  C_AKHmin <- min(as.numeric(as.vector(Trials[[i]]$angleC_AKH)), na.rm=TRUE)
  C_AKHrange <- C_AKHmax - C_AKHmin

  summaryList <- data.frame(paste(Trials[[i]]$BatTrial[1]), CAKsd, CAKmean, CAKmax,
    CAKmin, CAKrange,
                  C_AKHsd, C_AKHmean, C_AKHmax, C_AKHmin, C_AKHrange)
  summary <- rbind(summary, summaryList)
 }
 colnames(summary) = c("BatTrial", "CAKsd", "CAKmean", "CAKmax", "CAKmin",
    "CAKrange",
                "C_AKHsd", "C_AKHmean", "C_AKHmax", "C_AKHmin", "C_AKHrange")
 return(summary)
}

ErrorSummary <- function(data){
 Trials <- split(data, as.factor(data$BatTrial))
 x = length(Trials)
 error <- data.frame()
 for (i in 1:x){
  CalcarErrorMean <- mean(as.numeric(as.vector(Trials[[i]]$CalcarError)), na.rm=TRUE)
  HipKneeMean <- mean(as.numeric(as.vector(Trials[[i]]$HipKnee)), na.rm=TRUE)
  HipKneeSD <- sd(as.numeric(as.vector(Trials[[i]]$HipKnee)), na.rm=TRUE)
  KneeAnkleMean <- mean(as.numeric(as.vector(Trials[[i]]$KneeAnkle)), na.rm=TRUE)
  KneeAnkleSD <- sd(as.numeric(as.vector(Trials[[i]]$KneeAnkle)), na.rm=TRUE)
  errorlist <- data.frame(paste(Trials[[i]]$BatTrial[1]), CalcarErrorMean, HipKneeMean,
    HipKneeSD,
                KneeAnkleMean, KneeAnkleSD)
  error <- rbind(error, errorlist)
 }
 colnames(error) = c("BatTrial", "CalcarErrorMean", "HipKneeMean", "HipKneeSD",
    "KneeAnkleMean",
                "KneeAnkleSD")
 return(error)
}

#####################################################################
# Functions for applying angle calculations to kinematics data
#####################################################################
CalcarAngles<-function(data){
 # figure out how many rows (i.e., frames) I have to deal with
 # and initiate output
 x = length(data[,1])
```

```
  angles = data.frame()
  attach(data)

  #calculate angles for each row
  for (i in 1:x){
    # define vectors for each point from origin
    calcar = c(CalcarX[i], CalcarY[i], CalcarZ[i])
    ankle = c(AnkleX[i], AnkleY[i], AnkleZ[i])
    knee = c(KneeX[i], KneeY[i], KneeZ[i])
    hip = c(HipX[i], HipY[i], HipZ[i])
    #foot = c(FootX[i], FootY[i], FootZ[i])
    # define vectors between points
    AC =  calcar - ankle
    AK = knee - ankle
    KH = hip - knee
    KA = ankle - knee
    #AF = foot - ankle
    # define angles
    angleCAK = DotAngle(AC, AK)
    angleHKA = DotAngle(KH, KA)
    angleC_AKH = PlaneAngle(AC, KH, KA)
    #angleFAK = DotAngle(AF, AK)
    #angleF_AKH = PlaneAngle(AF, KH, KA)
    # bind them all together with the frame #
    anglelist = data.frame(paste(BatTrial[i]), paste(Bat[i]), Trial[i], Frame[i], Wingbeat[i],
      angleCAK, angleHKA, angleC_AKH)#, angleFAK, angleF_AKH)
    angles = rbind(angles, anglelist)
  }
  detach(data)
  colnames(angles) = c("BatTrial", "Bat","Trial", "Frame", "Wingbeat", "angleCAK",
      "angleHKA", "angleC_AKH")#, "angleFAK", "angleF_AKH")
  return(angles)
}

Error <- function(data){
  attach(data)
  info = data.frame(mean(CalcarError, na.rm=TRUE), mean(HipKnee, na.rm=TRUE),
      sd(HipKnee, na.rm=TRUE), max(HipKnee, na.rm=TRUE), min(HipKnee, na.rm=TRUE),
                mean(KneeAnkle, na.rm=TRUE), sd(KneeAnkle, na.rm=TRUE), max(KneeAnkle,
      na.rm=TRUE), min(KneeAnkle, na.rm=TRUE))
  colnames(info) = c("CalcarError", "HKmean", "HKsd", "HKmax", "HKmin",
                  "KAmean", "KAsd", "KAmax", "KAmin")
  detach(data)
  return(info)
}
```

```
################################
# Calculating speed and rise
################################
Speed <- function(pos1, pos2, fr1, fr2){
  dist_cm <- sqrt((pos2[1]-pos1[1])^2 + (pos2[2]-pos1[2])^2 + (pos2[3]-pos1[3])^2)
  dist_m <- dist_cm/100
  avesp <- dist_m/((fr2-fr1)/800)
  # Frame rate = 800 frames/sec
  return(avesp)
}

Rise <- function(pos1, pos2, posX, posY, posZ){
  # posX, Y and Z are points on the flight room floor digitized in one frame
  # below is text graphic representation:
  # PtX          PtZ
  #       PtY
  YX <- posX - posY
  YZ <- posZ - posY
  vec <- pos2 - pos1
  rise <- PlaneAngle(vec, YZ, YX)
  # the normal vector defined by the cross of YZ and YX should point *up* from the floor
  # thus, the angle b/t the vector of the body movement (vec) and the cross of the floor points
  # should be acute if the bat is rising and obtuse if the bat is falling
  # so a "rise" is a positive angle and a "fall" is a negative angle
  return(rise)
}

SpeedData <- function(data) {
  x = length(data[,1])
  speeds = data.frame()
  attach(data)

  for(i in 1:x){
    pos1 <- c(Body1x[i], Body1y[i], Body1z[i])
    pos2 <- c(Body2x[i], Body2y[i], Body2z[i])
    fr1 <- Fr1[i]
    fr2 <- Fr2[i]
    avesp <- Speed(pos1, pos2, fr1, fr2)
    posX <- c(PtX_x[i], PtX_y[i], PtX_z[i])
    posY <- c(PtY_x[i], PtY_y[i], PtY_z[i])
    posZ <- c(PtZ_x[i], PtZ_y[i], PtY_z[i])
    rise <- Rise(pos1, pos2, posX, posY, posZ)
    speedlist <- data.frame(paste(BatTrial[i]), paste(Bat[i]), Trial[i], avesp, rise)
    speeds <- rbind(speeds, speedlist)
  }
  detach(data)
```

```
  colnames(speeds) <- c("BatTrial", "Bat", "Trial", "Speed", "Rise")
  return(speeds)
}

################################
# Functions for finding angles
################################
# returns angles in degrees
# functions take in vectors between two points on the body
# A = ankle; C = calcar; K = knee; H = hip

# Angle between AC and AK or AF
DotAngle <- function(AC,AK){
  theta = acos(dot(AC,AK)/(mag(AC)*mag(AK)));
  degtheta = theta * (180/pi);
  return(degtheta)
}

# Angle between AC or AF and Plane AKH
PlaneAngle <- function(AC, KH, KA){
  # find vector normal to Plane AKH
  # as defined here, this will point dorsomedially for right bat hindlimb
  n = cross(KH, KA);
  # now find angle between calcar vector and Plane AKH normal
  a = acos(dot(n, AC)/(mag(n)*mag(AC)));
  # now find target angle->the angle between the plane and calcar vector
  # this will be positive for "dorsal"-pointing vectors
  # and negative for "ventral"-pointing vectors
  theta = (pi/2) - a;
  degtheta = theta * (180/pi);
  return(degtheta)
}

############################################
# Helper functions for working with vectors
############################################
cross <- function(a,b){
  x = a[2]*b[3] - a[3]*b[2];
  y = a[1]*b[3] - a[3]*b[1];
  z = a[1]*b[2] - a[2]*b[1];
  u = c(x,-y,z)
  return(u)
}

dot <- function(a,b){
  u = a[1]*b[1] + a[2]*b[2] + a[3]*b[3];
```

```
  return(u)
}

mag <- function(a){
  u = sqrt(a[1]^2 + a[2]^2 + a[3]^2);
  return(u)
}
```

CONCLUSION

How important is the calcar?

Unique anatomical structures are found throughout the kingdoms of life. Morphology is not perfectly deterministic for any organism. So why should the calcar be of interest to the broader biological community? Here, I have shown that the calcar is present throughout Chiroptera—over 1,400 species—in a wide variety of shapes, relative sizes, and tissue types. This anatomical variation potentially has functional consequences. I demonstrated that this anatomical diversity arose in a "early burst" of morphological evolution, mirroring the early phylogenetic and geographic radiation of bats. Lastly, I showed that motion of the calcar in at least one flight behavior in one species is not random—it exhibits biased movement in one direction over another. Collectively, these results strongly suggest that the calcar is of some functional importance to bats and may have helped shape their evolution by becoming an integral part of the bat bodyplan.

Implications for "Evolutionary Novelty"

Discrete, novel anatomical elements appear relatively rarely in the historical evolutionary record, and it is unclear what overall impact they have on altering the course of clade evolution. The findings of an early burst of calcar anatomical diversification and of functionally-relevant anatomical variation lend support to the idea that evolutionary novelty can, in some cases, precede and prompt adaptive radiations (i.e., the radiation of bats). The results of this dissertation particularly illuminate the evolution of the skeletal rods found in a variety of amniotes with membranes that glide or fly. The vertebrate skeleton is both labile and plastic. Studying these

enigmatic skeletal additions may help vertebrate biologists better understand the evolutionary capabilities of skeletal tissue and organs.

Future Work

The most obvious questions left unanswered by this dissertation are:
(1) Where does the calcar come from? – a question of homology and development; and
(2) What does the calcar do? – the still unanswered question of calcar function.

A complete story of calcar evolution cannot be told without an understanding of calcar development and how this novel skeletal organ arises from immediate ancestors that presumably did not possess one. Unfortunately, the fossil record leaves the evolutionary origin of bats completely opaque, so developmental studies are currently the only way to understand the origin of the calcar. Descriptive anatomical studies via histological sectioning, dissection, and CT scanning in embryonic, fetal, neonate, and juvenile bats are a necessary first step to understanding how the calcar initially forms in the embryo and how the its anatomical characteristics develop. Completing these studies in bats with different adult calcar morphologies could explain the developmental origin of calcar morphological variation. These anatomical investigations will then likely lead to rational, mechanistic theories of calcar development that can then be tested with molecular/immunochemical methods. One particular area of interest might be the affinity of the calcar to a prototypical sesamoid.

A somewhat related topic of potential interest is the amount of intraspecific variation in calcar morphology. As I examined calcars for this work, it often seemed to me (no more than a hunch) that the calcar might be more intraspecifically variable than other skeletal elements. Although I do not understand why this would be (inherent plasticity in cartilage vs. bone? Lack

of fixation in a population?) or what implications this might have for understanding calcar evolution, I do suspect that intraspecific and intrapopulational studies of calcar variation might reveal some important facts about skeletal biology and evolution.

Regarding calcar function, I suggest first completing standard functional morphology studies, in which the muscle and skeletal tissue anatomical parameters are used in a functional model of the calcar. The calcar is essentially a simple, rod-like structure and should be relatively straightforward to model. Functional morphology should provide clues to how the calcar muscles are physically capable of moving the membrane. These modeling results can then be tested in behavioral trials. Expanding the calcar kinematic analyses to more species and more behaviors might elicit useful information and provide additional support for functional diversification. The calcar might be particularly mobile as bats maneuver to capture food, an ecologically important task. The next obvious step is to conduct muscle physiology studies; i.e., determine if, when, and how calcar muscle activation affects calcar kinematics during ecologically-relevant behaviors.